ACS NANO

www.acsnano.org

ARTICLE

House Dust Mite Proteins Adsorb on Multiwalled Carbon Nanotubes Forming an Allergen Corona That Intensifies Allergic Lung Disease in Mice

Ryan D. Bartone, Logan J. Tisch, Judith Dominguez, Christine K. Payne, and James C. Bonner*

Cite This: *ACS Nano* 2024, 18, 26215−26232

Read Online

ACCESS | Metrics & More | Article Recommendations | Supporting Information

ABSTRACT: The increasing use of multiwalled carbon nanotubes (MWCNTs) could increase the risk of allergic lung disease in occupational or consumer settings. We previously reported that MWCNTs exacerbated allergic lung disease in mice induced by extract from house dust mites (HDM), a common cause of asthma in humans. Because MWCNTs avidly bind biomolecules to form protein coronas that can modify immunotoxicity, we hypothesized that exacerbation of allergic lung disease in mice caused by coexposure to MWCNTs and HDM extract was due to the formation of an allergen corona. In a first set of experiments, male and female C57BL/6J mice were coexposed to MWCNTs and HDM extract over 3 weeks compared to MWCNTs or HDM extract alone. In a second set of experiments, mice were exposed to pristine MWCNTs or MWCNTs with an HDM allergen corona (HDM-MWCNTs). HDM-MWCNTs were formed by incubating MWCNTs with HDM extract, where ∼7% of proteins adsorbed to MWCNTs, including Der p 1 and Der p 2. At necropsy, bronchoalveolar lavage fluid was collected from lungs to assess lactate dehydrogenase, total protein and inflammatory cells, while lung tissue was used for histopathology, qPCR, and Western blotting. Compared to MWCNTs or HDM extract alone, coexposure to MWCNTs and HDM extract or exposure to HDM-MWCNTs increased pathological outcomes associated with allergic lung disease (eosinophilia, fibrosis, mucous cell metaplasia), increased mRNAs associated with fibrosis (*Col1A1*, *Arg1*) and enhanced STAT6 phosphorylation in lung tissue. These findings indicated that exacerbation of HDM-induced allergic lung disease by MWCNTs is due to an allergen corona.

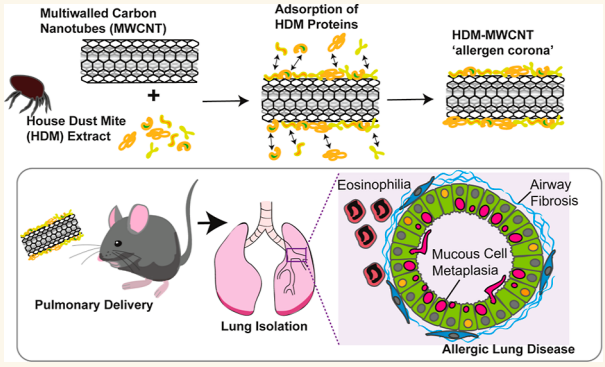

KEYWORDS: *carbon nanotubes, allergens, biocorona, lung, asthma*

Multiwalled carbon nanotubes (MWCNTs) are a widely used engineered nanomaterial (ENM) that are produced by chemical vapor deposition to form concentric cylinders of graphene.[1] Their durability, high tensile strength, flexibility, adsorption capability, and lightweight provide potential uses in a variety of applications, including catalysts, coatings, and additives to composite materials.[2,3] Because they can easily become airborne, the primary target organs for toxicological effects following exposure to MWCNTs are the lungs.[4,5] In experimental animal models, inhaled MWCNTs have been associated with a variety of disease outcomes including pulmonary fibrosis, cancer, and asthma.[6,7] With regards to asthma, we recently reported that pulmonary exposure to MWCNTs exacerbated house dust mite (HDM) extract-induced allergic lung disease, including eosinophilia, airway fibrosis and mucous cell metaplasia.[8] Elucidating the mechanisms through which coexposures to nanoparticles and allergens amplify allergic lung disease in mice is highly relevant to the exacerbation of asthma in humans.

Allergic asthma is a major human health issue worldwide that is due to a combination of genetic susceptibility and the host immune responses to a variety of environmental allergens derived from pollen, mold, or invertebrates, including the HDM *Dermatophagoides pteronyssinus*.[9−11] The immunologic

Received: June 13, 2024
Revised: August 26, 2024
Accepted: August 29, 2024
Published: September 11, 2024

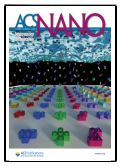

basis of asthma involves the uptake of inhaled allergens by dendritic cells, which then present the antigens to naïve T lymphocytes thereby causing polarization to a Th2 lymphocyte.[9,11] Th2 lymphocytes then produce the Th2 cytokines interleukin (IL)-4, IL-5, IL-9, and IL-13 that promote cellular and pathological outcomes associated with asthma, including eosinophilic lung inflammation, mucous cell metaplasia, airway fibrosis and airway hyperresponsiveness.[12,13] While allergens are a central cause of asthma, the inhalation of airborne particles from natural (e.g., wildfire smoke) or anthropogenic sources (e.g., diesel exhaust) exacerbate allergic asthma.[14,15] More recently, the emergence of nanotechnology has generated a variety of ENMs that have also been shown to exacerbate allergic lung disease in experimental animal models of asthma.[16,17] The mechanisms through which ENMs, or any other inhaled nanoparticle in the environment, exacerbate allergen-induced lung disease in a coexposure scenario remains unclear, but could involve a physical interaction between the nanoparticle and the allergen.

The adsorption of various proteins to nanoparticles to form a "biocorona" has become a well explored topic in the field of nanotoxicology and has been extensively reviewed.[18−23] When exposed to proteins in biological fluids (such as blood, plasma, or interstitial fluid), a protein corona forms on nanoparticles, modulating the cellular responses.[24,25] For example, the formation of a stable biocorona on carbon nanotubes using bovine serum albumin (BSA) as the protein source altered *Il6 mRNA* levels in rat endothelial cells and murine macrophages *in vitro*.[26,27] In addition to endogenous proteins, exogenous proteins and other biomolecules in the environment adsorb to nanoparticles to form a biocorona. For example, several types of allergens, including those from the HDM extract (e.g., Der p 1), form a corona on gold (Au) nanoparticles.[28] Moreover, in that study the proteolytic activity of the Der p 1 was enhanced when bound to the Au nanoparticles.[28] We recently reported that a variety of HDM extract proteins adsorb to MWCNTs and the dominant corona protein was Der p 2, an allergen strongly associated with allergic asthma.[29] Other studies have explored strategies using ENMs as allergen carriers in immunotherapy against allergies.[30,31] However, to our knowledge no studies have investigated the toxicological consequences of pulmonary exposure to ENMs with allergen coronas.

In this study, we aimed to explore the effects of MWCNTs with a HDM allergen corona (HDM-MWCNTs) on the pathogenesis of allergic airway disease in male and female mice. We hypothesized that the allergen corona is a mechanism through which MWCNTs exacerbate HDM extract-induced allergic lung disease in mice. Our findings demonstrate HDM proteins, including Der p 1 and Der p 2, adsorb to MWCNTs to form an allergen corona that significantly enhances allergic lung disease in mice similar to that seen with coexposure to MWCNTs and HDM extract. This work could have significant implications for human health due to the increasing use of MWCNTs and potential for exposure in occupational settings. Moreover, the data suggest that exposure scenarios where workers are coexposed MWCNTs and allergens could lead to the exacerbation of allergic asthma.

RESULTS

Pulmonary Coexposure to MWCNTs and HDM Extract Synergistically Enhance Allergic Lung Inflammation in Mice.

The physicochemical characteristics of the MWCNTs used in this study (NC7000 from Nanocyl, Inc.) were previously characterized.[32] Selected physicochemical characteristics of NC7000 MWCNTs are summarized in Table 1.

Table 1. Selected Physicochemical Characterization of NC7000 MWCNTs[a]

physicochemical characteristic	
amorphous carbon	4.68%
carbon[b]	92.05% (EDX); 97.8% (XPS)
oxygen	3.19% (EDX); 1.4 (XPS)
trace metals (ICP−MS)	4.43%
Al	0.54%
TE[c]	
avg. diameter (TEM)	12 nm
length (TEM, SEM)	1350 nm
BET surface area	24 m^2/g
pore volume	61 mL/g

[a]Adapted with permission from ref 32. Copyright 2020, Springer-Nature. [b]Carbon measured by EDX (energy dispersive X-ray analysis) or XPS (X-ray Photoelectron spectroscopy). [c]TE = transition elements (Co and Fe).

Transmission electron microscopy (TEM) demonstrated that these MWCNTs have a tangled morphology (Figure 1A). Using the sensitization and challenge protocol illustrated in Figure 1B, male and female C57BL/6 mice were exposed by oropharyngeal aspiration (OPA) a total of 6 times over a period of 3 weeks to the following treatments in 50 μL vehicle each dosing session: Dulbecco's phosphate buffered saline (DPBS) solution as the vehicle control, 0.5 mg/kg of MWCNTs (12.5 μg), 0.02 mg/kg of HDM extract (0.5 μg), or combination of MWCNTs and HDM extract. In this experiment, the cumulative dose of MWCNTs was 3 mg/kg and the cumulative dose of HDM extract was 0.12 mg/kg. In both male and female mice, coexposure to MWCNTs and HDM extract significantly increased total protein, lactate dehydrogenase (LDH) and total cell counts in BALF compared to the vehicle control group (Figure 1C−E). Photomicrographs of cytospin slides of BALF showed a marked increase in lung inflammatory cells that were primarily eosinophils (Figure 1F). Differential counting of BALF cells from cytospin slides showed that coexposure to MWCNTs and HDM extract significantly reduced the relative proportion of macrophages (Figure 1G), and this was due primarily to a marked increase in the numbers of eosinophils in both male and female mice (Figure 1H). MWCNT exposure alone produced a marginal yet significant increase in the number of neutrophils in BALF in both sexes (Figure 1I). The absolute numbers of macrophages, eosinophils, and neutrophils in each treatment group from which the percentage of each cell type was derived is shown in Figure S1.

Coexposure to MWCNTs and HDM Extract Modulate the Pathogenesis of Allergic Lung Disease in Mice.

Lung sections of male and female mice were prepared and stained for histopathology. Lung sections were stained with hematoxylin and eosin (H&E) to assess inflammation in the lungs. The relatively low dose of HDM extract used in this study did not result in any significant increase in focal inflammation in either male or females (Figure 2A). MWCNTs alone caused focal inflammation in the alveolar region along with granuloma formation (Figure 2A). Inflammation and granulomas were

https://doi.org/10.1021/acsnano.4c07893
ACS Nano 2024, 18, 26215−26232

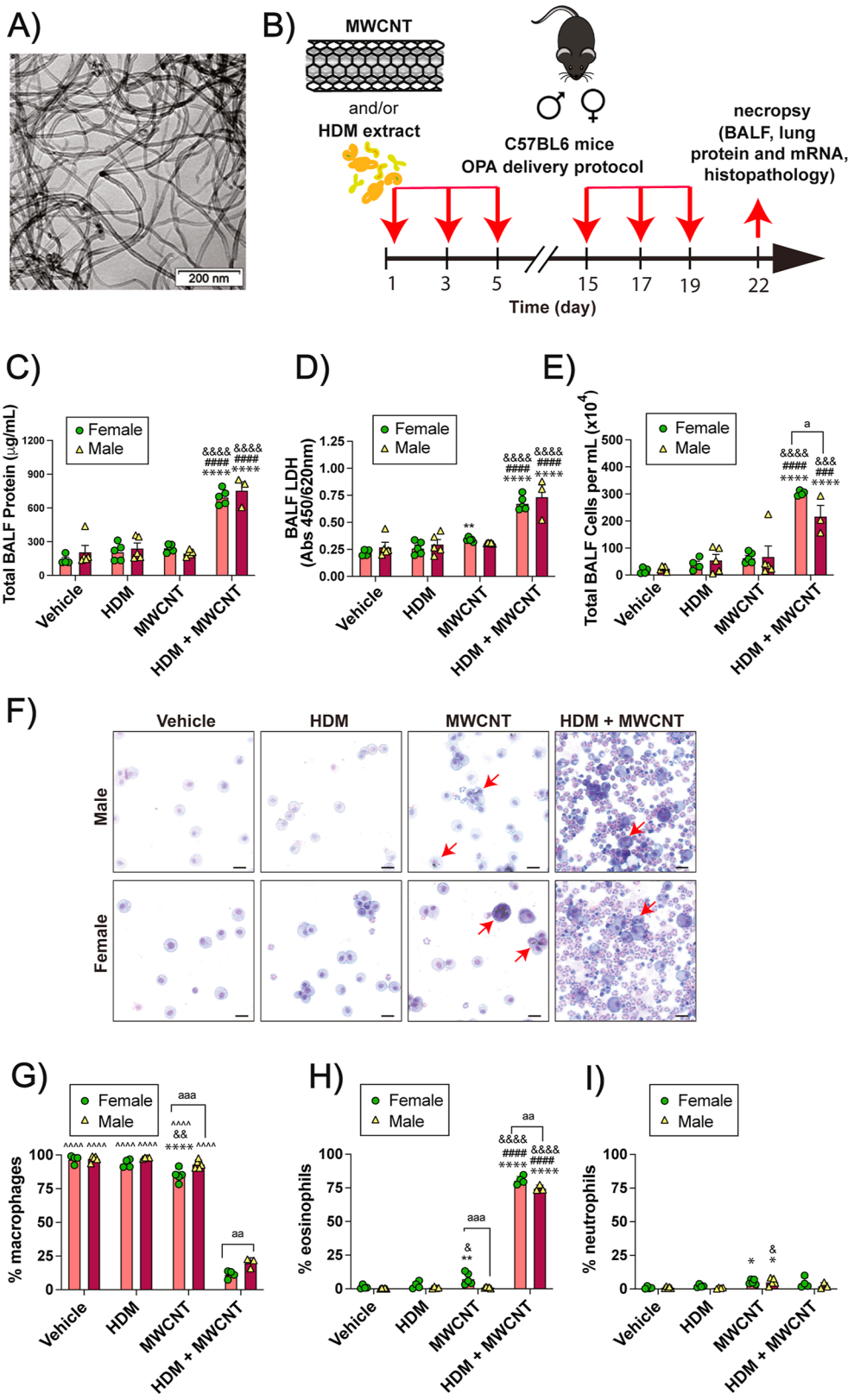

Figure 1. Cellularity and biomarkers of lung injury in BALF collected from mice exposed to HDM extract, MWCNTs or both. (A) TEM image of NC7000 MWCNTs. (B) Illustration of the exposure protocol using oropharyngeal aspiration of MWCNT and/or HDM extract. (C–E) Total protein, LDH and total cell counts in BALF. (F) Cytospin images from BALF showing eosinophilic inflammation after coexposure to MWCNTs and HDM extract. Red arrows indicate macrophages with MWCNT inclusions. Black bars = 10 μm. (G–I) Differential cell counts from cytospins showing macrophages, eosinophils, and neutrophils. **$p < 0.01$, ****$p < 0.0001$ compared to vehicle; $^{\#\#\#}p < 0.001$, $^{\#\#\#\#}p < 0.0001$ compared to MWCNT; $^{\&}p < 0.05$, $^{\&\&}p < 0.01$, $^{\&\&\&}p < 0.001$, $^{\&\&\&\&}p < 0.0001$ compared to HDM; $^{\wedge\wedge\wedge\wedge}p < 0.0001$ compared to HDM + MWCNT; $^{a}p < 0.05$, $^{aa}p < 0.01$, $^{aaa}p < 0.001$ between sexes determined by two-way ANOVA with Tukey's post hoc analysis.

https://doi.org/10.1021/acsnano.4c07893
ACS Nano 2024, 18, 26215–26232

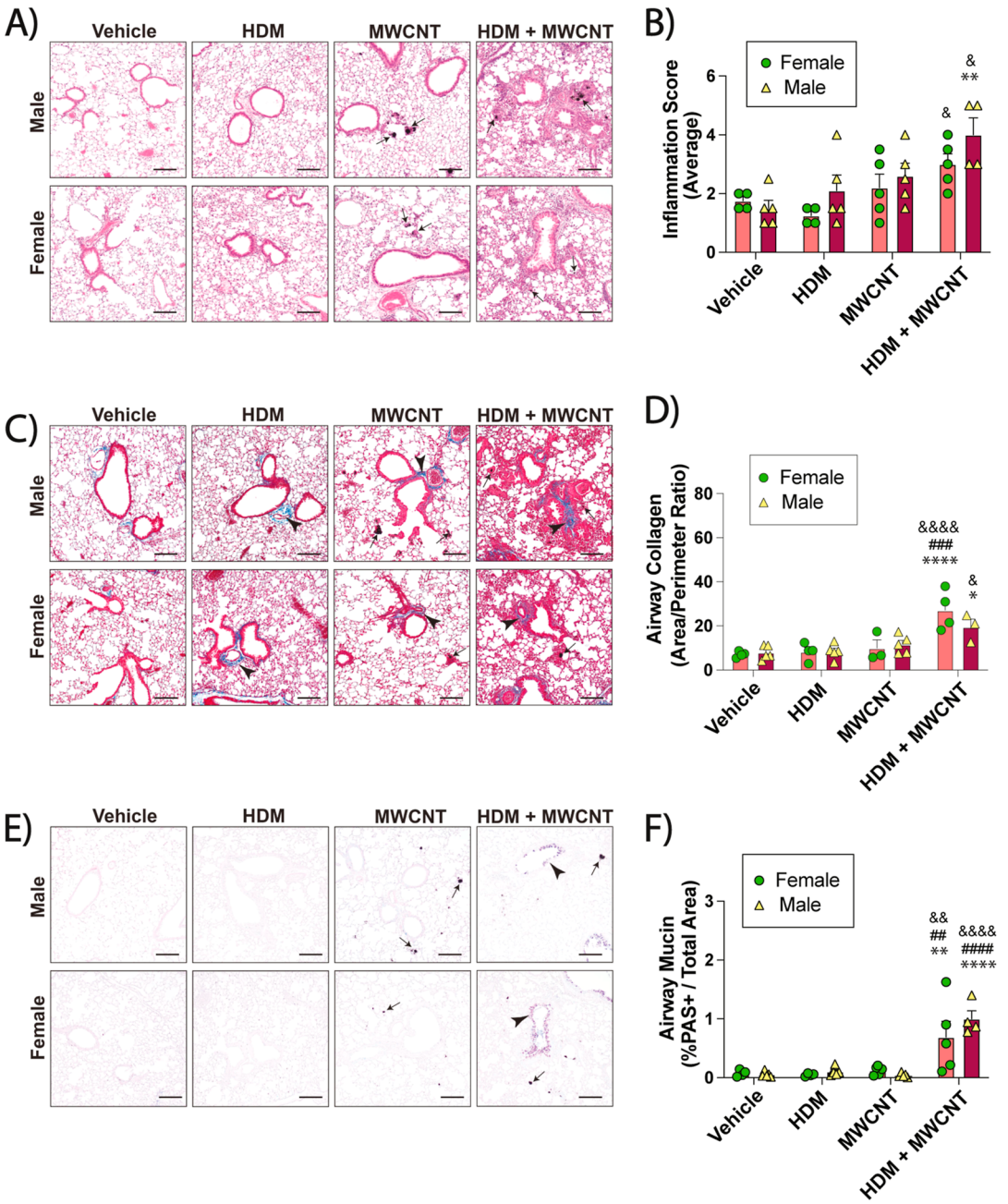

Figure 2. Allergic lung disease in male and female mice exposed to HDM extract, MWCNTs or both. (A) Representative images of H&E-stained lungs sections. Arrows indicate MWCNTs. Black bars = 100 μm. (B) Inflammation scores derived from H&E-stained sections from all animals. (C) Representative images of Masson's trichrome-stained lung sections showing blue-stained collagen (arrowheads). Black arrows indicate MWCNTs. Black bars = 100 μm. (D) Quantification of trichrome-positive airway collagen from all animals using area-perimeter ratio method. (E) Representative images of AB-PAS -stained lung tissue sections showing purple PAS + mucins (arrowheads). Arrows indicate MWCNTs. Black bars = 100 μm. (F) Morphometric quantification of AB-PAS + airway mucin. $^{*}p < 0.05$, $^{**}p < 0.01$, $^{****}p < 0.0001$ compared to vehicle treatment; $^{\#\#}p < 0.01$, $^{\#\#\#}p < 0.001$, $^{\#\#\#\#}p < 0.0001$ when compared to MWCNT treatment; $^{\&}p < 0.05$, $^{\&\&}p < 0.01$, $^{\&\&\&\&}p < 0.0001$ when compared to HDM treatment as determined by two-way ANOVA with Tukey's post hoc analysis.

further increased in the lungs of mice exposed to the coexposures of MWCNTs and HDM extract (Figure 2A). The inflammation score was increased in both male and female mice treated with coexposure compared to MWCNTs alone, HDM alone, or vehicle (Figure 2B). The evaluation of fibrosis in the lungs of male and female mice was conducted using Masson's trichrome staining. Morphometric analysis of photomicrographs from trichrome-stained lung sections showed that the coexposure of MWCNTs and HDM extract increased airway fibrosis in the lungs of both male and female mice as compared to MWCNTs alone, HDM alone, or vehicle (Figure 2C). Fibrosis was quantified by measuring the area-perimeter ratio of trichrome-positive collagen around airways (Figure 2D). Photomicrographs of AB-PAS-stained lung sections showed a marked increase in mucous cell metaplasia in the airways of male and female mice after coexposure to HDM extract and MWCNTs, but not any of the other treatment groups (Figure 2E). Quantitative morphometry showed significant increases in the percentage of AB-PAS positive stained cells based on the area of respective airways in both

https://doi.org/10.1021/acsnano.4c07893
ACS Nano 2024, 18, 26215−26232

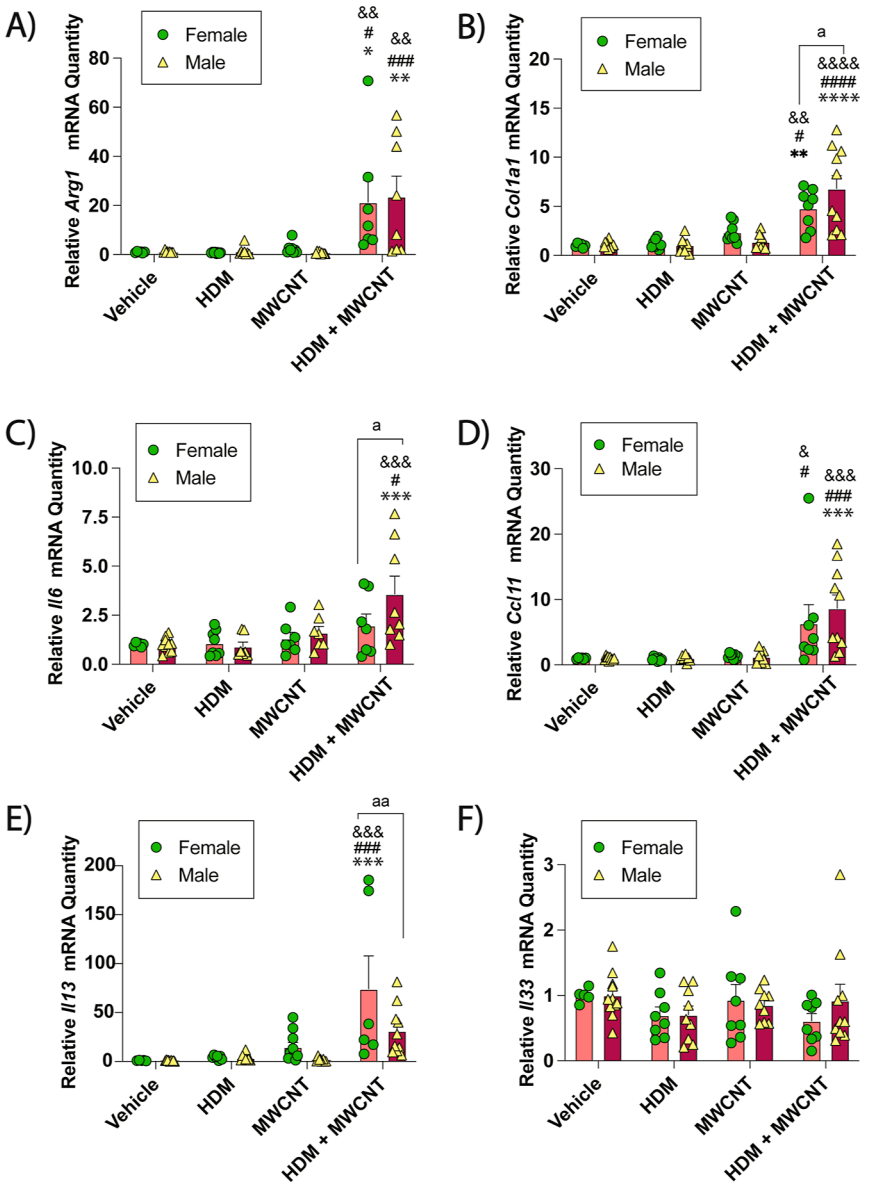

Figure 3. qRT-PCR of cytokines and cell signaling mediators in the lungs of male and female mice exposed to MWCNTs with or without HDM extract. (A) *Arg-1* mRNA. (B) *Col1a1* mRNA. (C) *Il6* mRNA.(D) *Ccl11* mRNA. (E) *Il13* mRNA. (F) *Il33* mRNA. $^{*}p < 0.05$, $^{**}p < 0.01$, $^{***}p < 0.001$, $^{****}p < 0.0001$ compared to vehicle treatment; $^{\#}p < 0.05$, $^{\#\#\#}p < 0.001$, $^{\#\#\#\#}p < 0.0001$ when compared to MWCNT treatment; $^{\&\&}p < 0.01$, $^{\&\&\&}p < 0.001$, $^{\&\&\&\&}p < 0.0001$ when compared to HDM treatment; $^{a}p < 0.05$ or $^{aa}p < 0.01$ when comparing sexes as determined by two-way ANOVA with Tukey's post hoc analysis.

male and female coexposure groups compared to the other treatment groups (Figure 2F).

MWCNT and HDM Extract Coexposures Exacerbate mRNA Expression of Pro-Inflammatory and Pro-Fibrotic Mediators. Gene expression analysis via qRT-PCR revealed significantly increased *Arg-1* mRNA expression in male or female mice coexposed to MWCNTs and HDM extract (Figure 3A). Coexposure to MWCNTs and HDM extract also increased *Col1a1* mRNA, which encodes collagen proteins that contribute to lung fibrosis (Figure 3B). Pro-inflammatory cytokine mRNAs *Il6*, *Ccl11*, *Il13* and *Il33* were also measured. Coexposure to HDM extract and MWCNTs significantly increased *Il6* mRNA in male mice but not female mice (Figure 3C). Gene expression of *Ccl11*, a primary eosinophil chemokine, was significantly increased by coexposure to HDM extract and MWCNTs in both male and female mice, yet no sex differences were observed (Figure 3D). Coexposure to HDM extract and MWCNTs significantly increased *Il13* mRNA in female mice but not male mice (Figure 3E), whereas coexposure did not significantly change *Il33* mRNA (Figure 3F).

MWCNT and HDM Extract Coexposure Increases the Phosphorylation of STAT6 in Lung Tissue. Lung protein lysates were analyzed by Western blot analysis to measure phosphorylated STAT6 and total STAT6 protein levels in mice exposed to MWCNTs, HDM extract, or a combination of both (Figure 4). Western blots of 4 male or female mice for each treatment group are shown in Figure 4A and semiquantitative densitometry of the p-STAT6 signal from each group of mice normalized to either total STAT6 or β-actin is shown in Figure 4B. The original uncropped Western blot data are shown in Supporting Information Figure S2. Coexposures of HDM

https://doi.org/10.1021/acsnano.4c07893
ACS Nano 2024, 18, 26215−26232

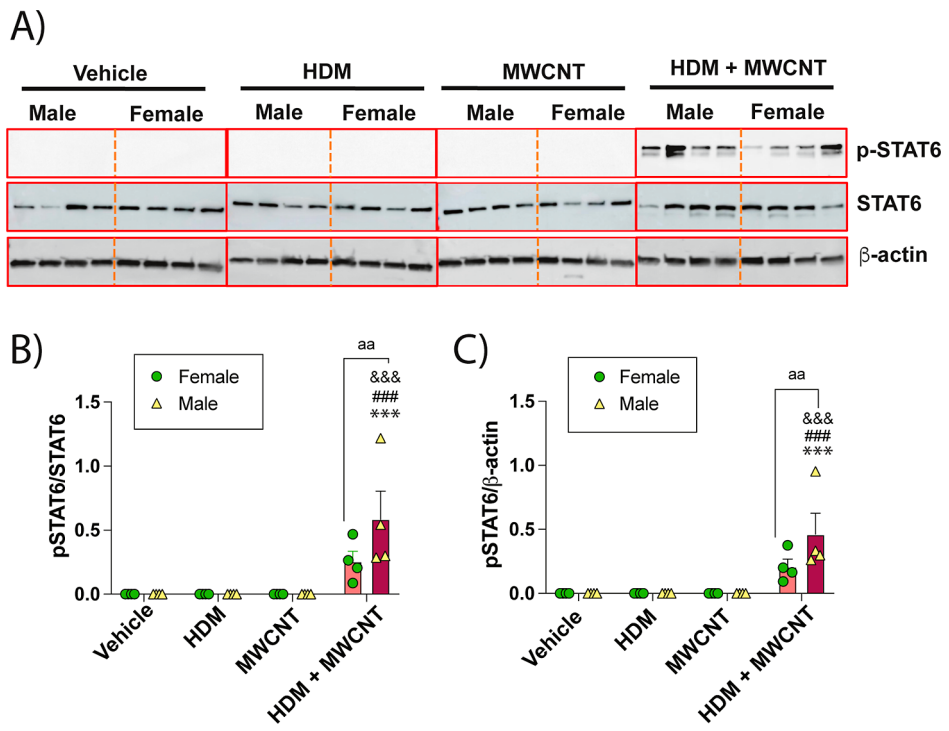

Figure 4. (A) Western blots of whole lung lysates from male and female mice exposed to vehicle, HDM extract, MWCNTs, or both. Each lane represents an individual animal. (B) Densitometry of p-STAT6 normalized against total STAT6 or β-Actin. $^{***}p < 0.001$ compared to vehicle treatment; $^{\#\#\#}p < 0.001$ compared to MWCNT treatment; $^{\&\&\&}p < 0.001$ compared to HDM treatment; $^{aa}p < 0.01$ comparing sexes as determined by two-way ANOVA with Tukey's post hoc analysis.

extract and MWCNTs increased p-STAT6 compared to other treatment groups (Figure 4A). Densitometric analysis showed that male mice exhibited higher levels of p-STAT6 compared to female mice when normalized to either total STAT6 or β-actin (Figure 4B).

Key Allergenic Proteins Found in HDM Extract Adsorb to the Surface of MWCNTs to form a HDM Allergen Corona. To characterize the HDM-MWCNT allergen corona, cell-free samples were prepared and evaluated by BCA and Western blot analysis. Figure 5A depicts the process by which the HDM-MWCNTs were formed, and details are described in the Method section. We previously reported the results of a proteomic analysis using liquid chromatography with tandem mass spectrometry (LC−MS/MS) to show the normalized abundance (% of total protein) of the top 10 proteins identified in HDM extract and the HDM corona formed on MWCNTs (HDM-MWCNTs).[29] The same lot number of HDM extract was used for proteomic analysis and animal exposures. Figure 5B shows the normalized abundance (% of total protein) of the top 10 proteins identified in HDM extract and the HDM-MWCNTs from the proteomic analysis. The proteomic analysis identified both Der p 1 and Der p 2 in the HDM-MWCNT corona and showed that der p 2, but not Der p 1, was enriched (Figure 5B). Total protein quantification via BCA showed that approximately 7% of original concentration of HDM extract was adsorbed on the surface of the MWCNTs following incubation and rinsing (Figure 5C). Two well-known HDM proteins that are linked to asthma in humans, Der p 1 and der p 2, were previously identified in the HDM-MWCNTs by proteomics[29] and were therefore measured and further quantified by Western blot analysis (Figure 5D,E). Compared to the initial concentration of HDM extract, it was found that Der p 2 protein was significantly enriched upon the surface of MWCNTs (Figure 5D). Der p 1 was also identified as a corona protein but was not enriched compared to the initial concentration in HDM extract (Figure 5E). Dynamic light scattering (DLS) was performed to determine whether the HDM corona altered the agglomeration and dispersion of MWCNTs in aqueous media (DPBS). DLS showed that HDM-MWCNTs had decreased hydrodynamic diameter and polydispersity index (PDI) compared to pristine MWCNTs, but not to a significant extent (Figure S3).

Pulmonary Exposure to HDM-MWCNT Allergen Corona Mimics HDM Extract and MWCNT Coexposure Treatment Responses in Mice. As illustrated in Figure 6A, mice were exposed by OPA a total of 6 times over a period of 3 weeks to the following treatments in 50 μL vehicle for each dosing session: DPBS solution as the vehicle control, 0.5 mg/kg MWCNTs (12.5 μg for males; 10 μg for females), or HDM-MWCNTs prepared by the incubation of MWCNTs with HDM extract described in Methods and Materials. Both male and female mice had significantly higher total BALF protein after exposure to the HDM-MWCNTs compared to pristine MWCNTs (Figure 6B). Female mice also had significantly higher total BALF protein than male mice after exposure to HDM-MWCNTs (Figure 6B). A significantly higher level of LDH in the BALF of male mice was observed after exposure to MWCNTs alone when compared to the vehicle treatment, yet exposure to HDM-MWCNTs did not further increase LDH levels compared to pristine MWCNTs (Figure 6C). Moreover, female mice exposed to HDM-MWCNTs had a significant increase in LDH compared to control treatments and was also significantly higher than male mice exposed to HDM-MWCNTs. Furthermore, both male and female mice exposed to HDM-MWCNTs had a significantly higher total BALF cell

https://doi.org/10.1021/acsnano.4c07893
ACS Nano 2024, 18, 26215−26232

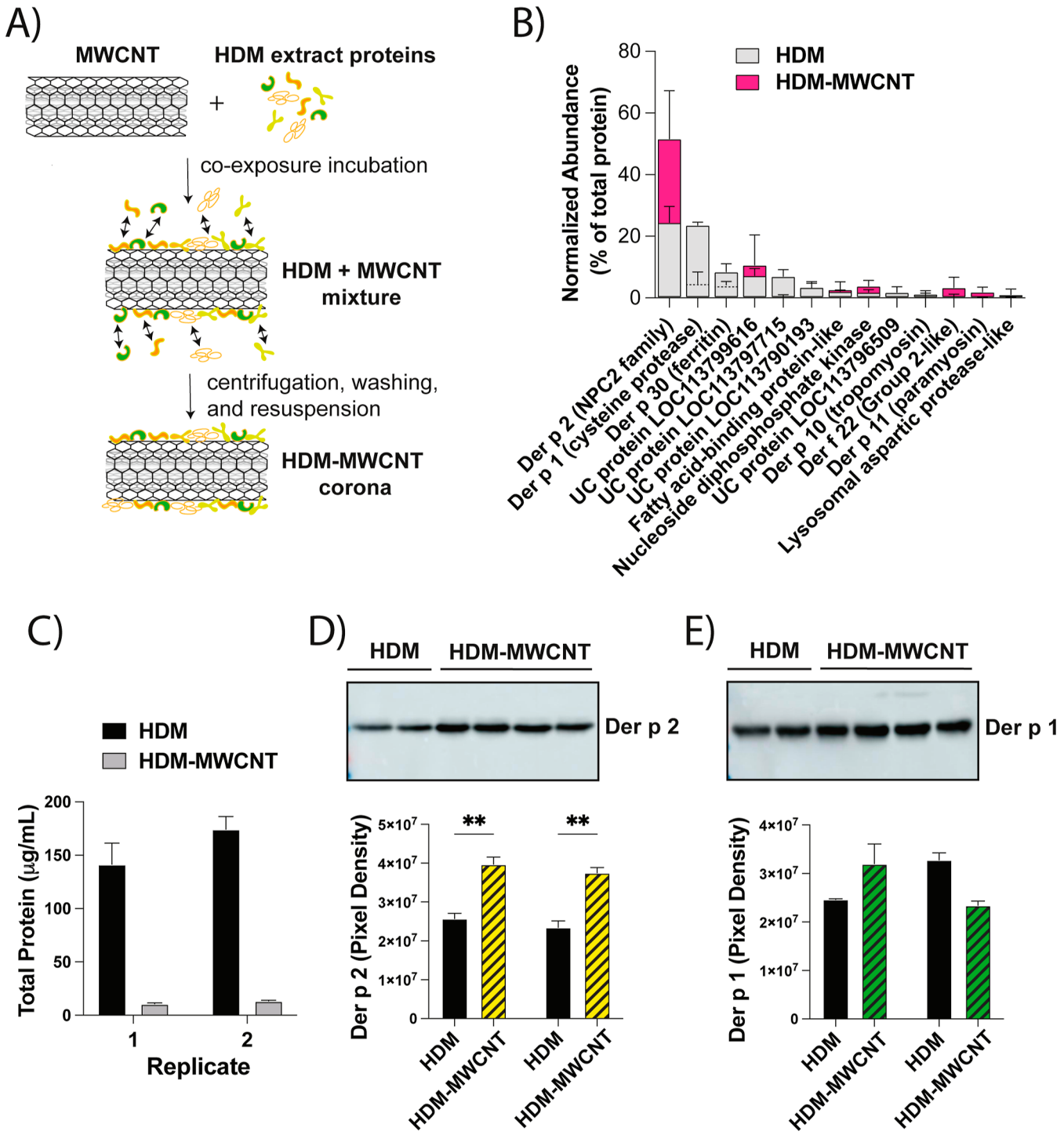

Figure 5. Characterization of the HDM-MWCNT allergen corona. (A) Schematic showing the preparation of MWCNT-HDM coronas (see details in Methods). (B) Normalized abundance (% of total protein) of the top-10 proteins identified in HDM extract and the HDM corona formed on MWCNTs (HDM-MWCNT) identified by proteomic analysis using liquid chromatography with tandem mass spectrometry (LC–MS/MS). UC denotes uncharacterized protein. Adapted with permission from ref 29, Table S3. Copyright 2024, Royal Society of Chemistry. (C) Total protein in HDM extract (HDM) or extracted from HDM-MWCNT corona with lysis buffer. (D,E) Western blots of Der p 2 and Der p 1 extracted from HDM-MWCNTs along with densitometry from two replicates. **$p < 0.01$ between HDM extract and HDM-MWCNTs.

count than either the MWCNT treatment group or the vehicle control group, while treated female mice had significantly higher cell counts than the male mice (Figure 6D). Cytospin slide images of BALF cells revealed a marked increase in the number of lung inflammatory cells after exposure to HDM-MWCNTs (Figure 6E). Differential cell counting to quantify the relative proportion of cell types showed that the percentage of alveolar macrophages significantly decreased after exposure to the HDM-MWCNTs (Figure 6F) and this was due primarily to an increase in the relative numbers of eosinophils (Figure 6G). Neutrophil cell counts showed no differences among treatment groups; however, there was a significant

https://doi.org/10.1021/acsnano.4c07893
ACS Nano 2024, 18, 26215−26232

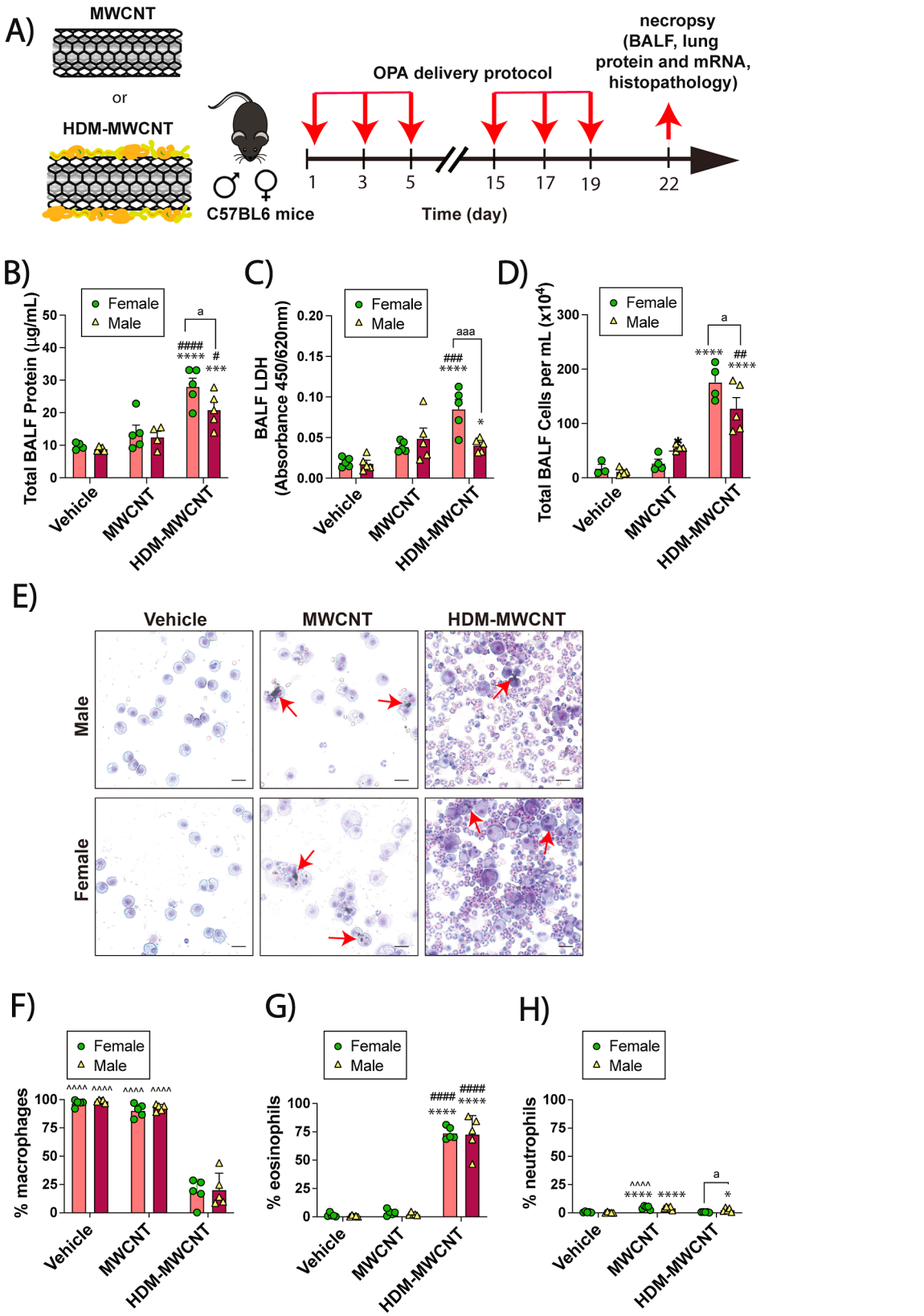

Figure 6. Cellularity analysis and biomarkers of lung injury in BALF collected from mice exposed to MWCNTs or HDM-MWCNTs. (A) Schematic of the exposure protocol in mice using oropharyngeal aspiration (OPA) of MWCNTs or HDM-MWCNTs. (B–D) Total protein, LDH and total cell counts in BALF. (E) Cytospin images from BALF from mice showing eosinophilic inflammation after exposure to HDM-MWCNTs. Red arrows indicate macrophages with MWCNT inclusions. Black bars = 10 μm. (F–H) BALF differential cell counts showing macrophages, eosinophils and neutrophils. *p < 0.05, ****p < 0.0001 compared to vehicle treatment; $^{\#\#\#\#}p$ < 0.0001 when compared to MWCNT treatment; $^{\wedge\wedge\wedge\wedge}p$ < 0.0001 when compared to MWCNT-HDM corona treatment; ^{a}p <0.05 when comparing sexes as determined by two-way ANOVA with Tukey's post hoc analysis.

https://doi.org/10.1021/acsnano.4c07893
ACS Nano 2024, 18, 26215–26232

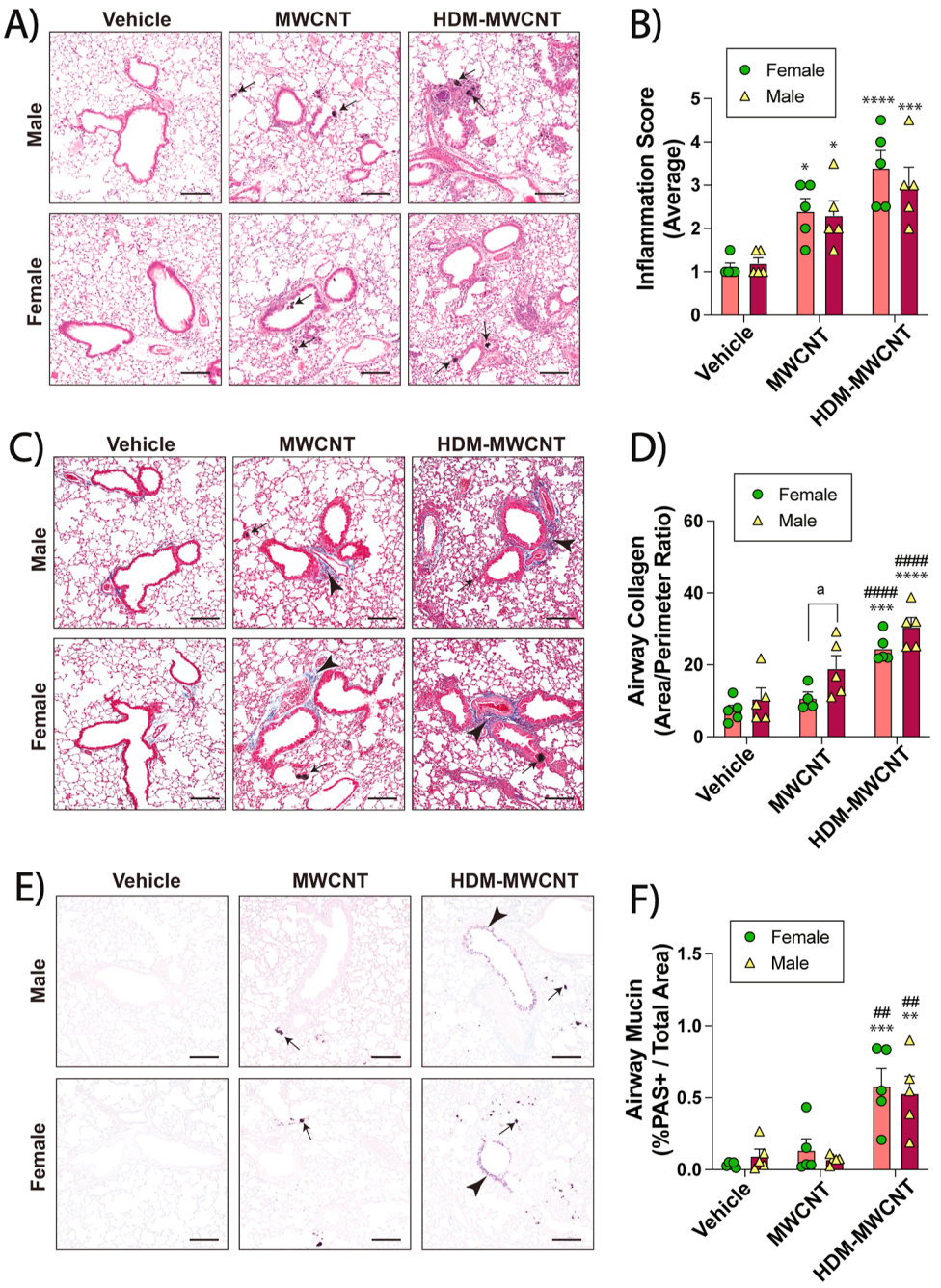

Figure 7. Allergic lung disease in mice exposed to MWCNTs or HDM-MWCNTs. (A) Representative images of H&E-stained lungs sections. Arrows indicate MWCNTs. Black bars = 100 μm. (B) Inflammation scores derived from H&E-stained lung sections from all animals. (C) Representative images of Masson's trichrome-stained lung sections showing blue-stained collagen (arrowheads). Black arrows indicate MWCNTs. Black bars = 100 μm. (D) Quantification of trichrome-positive airway collagen from all animals using area-perimeter ratio method. (E) Representative images of AB-PAS- stained lung tissue sections showing purple PAS + mucins (arrowheads). Arrows indicate MWCNTs. Black bars = 100 μm. (F) Morphometric quantification of AB-PAS + airway mucin. *$p < 0.05$, **$p < 0.01$, ***$p < 0.001$, ****$p < 0.0001$ compared to vehicle; $^{\#\#}p < 0.01$, $^{\#\#\#\#}p < 0.0001$ compared to MWCNT; $^{a}p < 0.05$ comparing sexes as determined by two-way ANOVA with Tukey's post hoc analysis.

increase when comparing male mice to female mice after HDM-MWCNT exposure (Figure 6H). The absolute numbers of macrophages, eosinophils, and neutrophils in each treatment group from which the percentage of each cell type was derived is shown in Figure S4.

HDM-MWCNT Allergen Corona Mediates the Pathogenesis of Allergic Lung Disease in Mice. Lung histopathology sections from male and female mice were prepared and stained with hematoxylin and eosin (H&E) to highlight inflammation in the lungs. Pristine MWCNTs or HDM-MWCNTs caused focal inflammation in the alveolar region along with some granuloma formation, with HDM-MWCNTs producing more severe pathology (Figure 7A). Semiquantitative scoring of inflammation scoring on a scale of 1−5 showed that both male and female mice treated with MWCNTs had a significant increase in lung inflammation that was further increased by HDM-MWCNTs (Figure 7B). The evaluation of fibrosis in the lungs of mice was conducted using

https://doi.org/10.1021/acsnano.4c07893
ACS Nano 2024, 18, 26215−26232

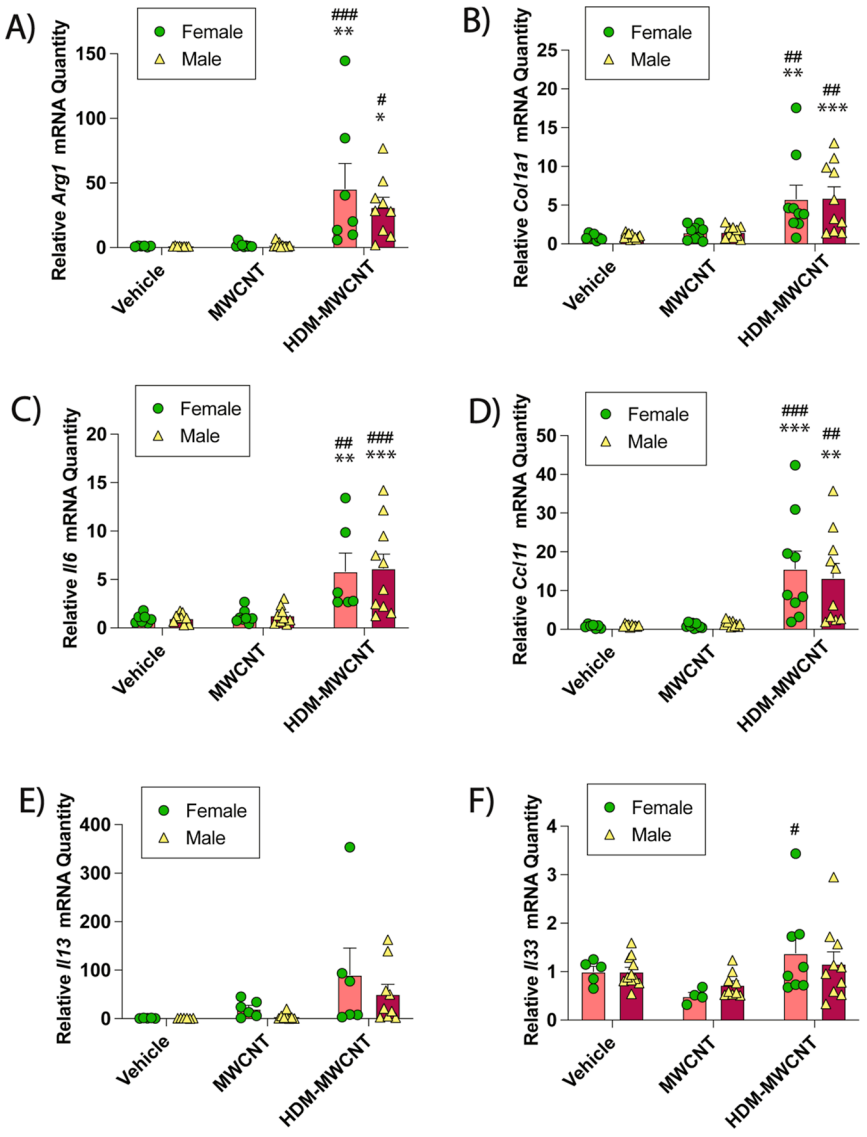

Figure 8. qRT-PCR of cell signaling mediators in the lungs of male and female mice exposed to MWCNTs or HDM-MWCNTs. (A) *Arg1* mRNA. (B) *Col1a1* mRNA. (C) *Il6* mRNA. (D) *Ccl11* mRNA. (E) *Il13* mRNA. (F) *Il33* mRNA. $^{*}p < 0.05$, $^{**}p < 0.01$, $^{***}p < 0.001$ compared to vehicle treatment; $^{\#}p < 0.05$, $^{\#\#}p < 0.01$, $^{\#\#\#}p < 0.001$ compared to MWCNT treatment as determined by two-way ANOVA with Tukey's post hoc analysis.

Masson's trichrome staining followed by morphometry of trichrome-positive airway collagen using the area-perimeter ratio method. Photomicrographs of trichrome-stained lung sections are shown in Figure 7C. Semiquantitative morphometry using the area-perimeter method revealed that exposure to HDM-MWCNTs increased airway fibrosis in the lungs of both male and female mice as compared to pristine MWCNTs or vehicle (Figure 7D). Photomicrographs of AB-PAS-stained lung sections showed a marked increase in mucous cell metaplasia in the airways of male and female mice exposed to HDM-MWCNTs, but not pristine MWCNTs or vehicle control (Figure 7E). Quantitative morphometry showed that both male and female mice exposed to HDM-MWCNTs had greater airway mucin compared to pristine MWCNTs or vehicle (Figure 7F).

The HDM-MWCNT Allergen Corona Mediates Pro-Fibrotic and Pro-Inflammatory Mediator Gene Expression. Lung lysates were collected from male and female mice that were exposed to a vehicle solution, pristine MWCNTs, or MWCNT-HDMs. The level of *Arg1* mRNA was not significantly increased by pristine MWCNTs compared to the vehicle control in either male or female mice. However, *Arg1* mRNA expression in male and female mice exposed to HDM-MWCNTs was significantly increased by > 20-fold (Figure 8A). *Col1a1* mRNA was also significantly increased in the lungs of male and female mice exposed to the HDM-MWCNTs (Figure 8B). In addition, mRNAs encoding the pro-inflammatory mediators *Il6* and *Ccl11* were significantly increased after exposure to HDM-MWCNTs in lung tissue from male and female mice, but not with pristine MWCNTs (Figure 8C–D). HDM-MWCNTs significantly increased *Il13* mRNA in female mice but not male mice (Figure 8E). Additionally, HDM-MWCNTs increased *Il33* mRNA in female mice but not in male mice (Figure 8F).

The HDM-MWCNT Allergen Corona Increases the Phosphorylation of STAT6 in the Lungs of Mice. Protein samples were also collected from the lung lysates from male and female mice after exposures to a vehicle control,

https://doi.org/10.1021/acsnano.4c07893
ACS Nano 2024, 18, 26215−26232

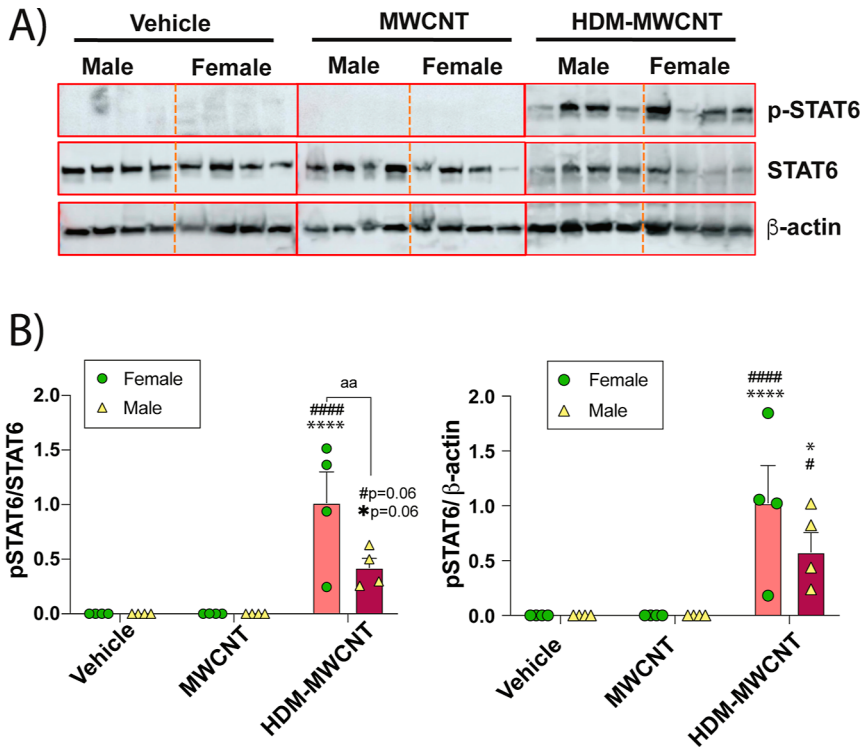

Figure 9. (A) Western blots of p-STAT6, STAT6 and l3-actin in lung lysates from mice exposed to MWCNTs or HDM-MWCNTs. (B) Quantitative densitometry of pSTAT6 normalized against total STAT6 or p-actin. **$p < 0.01$, ****$p < 0.0001$ compared to vehicle; $^{\#}p < 0.05$, $^{\#\#}p < 0.01$, $^{\#\#\#\#}p < 0.0001$ when compared to MWCNT treatment; $^{aa}p < 0.01$ when comparing sexes as determined by two-way ANOVA with Tukey's post hoc analysis.

MWCNTs, or HDM-MWCNTs and evaluated by Western blot analysis for phosphorylation of STAT6 relative to total STAT6. Western blots from 4 male and 4 female mice evaluated from each treatment group are shown in Figure 9A. The original uncropped Western blots are shown in Figure S5. HDM-MWCNTs increased p-STAT6 in lung tissue from both male and female mice whereas pristine MWCNTs did not (Figure 9A). Semiquantitative densitometry confirmed that HDM-MWCNTs caused a significant increase in p-STAT6 protein compared to a vehicle or pristine MWCNTs in female mice when normalized to total STAT6 or β-actin. Male mice also had elevated p-STAT6 after exposure to HDM-MWCNTs when normalized to β-actin and was nearly significant ($p = 0.06$) when normalized to total STAT6 (Figure 9B).

DISCUSSION

We previously reported that the allergic lung response to relatively low doses of HDM extract is highly amplified by coexposure to MWCNTs in male C57BL6 mice.[8] The allergic lung response was characterized by eosinophilic lung inflammation, airway fibrosis and mucous cell metaplasia. In the present study, we first confirmed that coexposure to MWCNTs and HDM extract synergistically increased eosinophilic lung inflammation compared to MWCNTs or HDM extract alone in both male and female mice. However, the underlying mechanism through which MWCNTs exacerbated HDM extract-induced allergic lung disease remained unknown. Recently, we demonstrated that a variety of HDM proteins adsorb to MWCNTs to form an allergen corona and Der p 2 was identified as a dominant protein that was enriched in the allergen corona.[29] In the current study, we discovered that all aspects of allergic lung disease, including eosinophilia, airway fibrosis and mucous cell metaplasia, were significantly enhanced by HDM-MWCNTs compared to pristine MWCNTs. Therefore, our findings demonstrate that the allergen corona is a key mechanism through which MWCNTs exacerbate HDM extract-induced allergic lung disease in mice. To our knowledge, the current study is the only report assessing the pathological consequences of a nanoparticle-HDM allergen corona delivered to the lungs of mice.

The enhanced allergic lung inflammatory response to MWCNTs with HDM corona in mice was almost as robust as that achieved with coexposure to HDM extract and MWCNTs, even though only a small fraction of the HDM extract protein (~7%) adsorbed to MWCNTs to form a corona. We previously reported that Der p 2 is enriched on the surface of HDM-MWCNTs as part of the allergen corona.[29] For example, Der p 2 comprised ~25% of the total protein in HDM extract yet made up ~52% of the total protein in the HDM-MWCNTs (Figure 5B). This finding has important implications for allergic airway disease since Der p 2 is the major human allergen in HDM extract that is linked to the pathogenesis of asthma.[33] Studies with mice also support a role for Der p 2 as a causative agent of HDM extract that produces pathological outcomes of allergic lung disease. For example, the intratracheal instillation of Der p 2 into the lungs of mice produced eosinophilic inflammation, mucous cell metaplasia and airway fibrosis.[34] All of these pathological outcomes were observed in the present study after oropharyngeal aspiration of HDM-MWCNTs or coexposure to HDM extract and MWCNTs. Moreover, der p 2-derived peptide immunotherapy abrogates asthma-related features in mice exposed to HDM extract.[35] These findings support Der p 2 as a major allergen in

https://doi.org/10.1021/acsnano.4c07893
ACS Nano 2024, 18, 26215−26232

HDM extract that mediates allergic lung disease. The reason for enrichment of Der p 2 in HDM-MWCNTs is unknown but could be due, at least in part, to the hydrophobicity of MWCNTs. We previously reported that the MWCNTs used in this study have a negative zeta potential in aqueous media.[32] Hydrophobicity has been linked to negative zeta potential and is a major factor that mediates cellular uptake of pristine MWCNTs.[36] Der p 2 also binds to hydrophobic molecules. For example, Der p 2 has been identified as a major cholesterol binding protein.[37] Der p 1 is another major human allergen in HDM extract yet was identified in the HDM-MWCNT allergen corona at relatively low abundance.[29] In the present study, we were able to demonstrate both Der p 1 and Der p 2 in the HDM-MWCNTs by Western blot analysis. It is noteworthy that we used the same source and lot number of HDM extract as described previously.[29] This is an important issue, since the pathologic and physiologic response to HDM extract exposure in mice is dependent on lot characteristics.[38] While Der p 2 is likely the most important HDM allergen identified in the HDM-MWCNTs, other proteins that we previously identified by proteomic analysis such as der p 30 (ferritin), der p 36 (C2 domain containing protein), and Der p 1 (cysteine protease), could be contributory allergic lung disease.

The mechanism through which HDM-MWCNTs amplify allergic lung disease in mice remains to be elucidated. As mentioned above, Der p 2 was previously identified as the most abundant HDM protein in the allergen corona and this may provide an explanation for the increased inflammatory responses in mice exposed to the HDM-MWCNTs.[29] Der p 2 is a functional mimic of the toll-like receptor 4 (TLR4) cofactor MD-2 that drives lung conventional DC activation and airway inflammation.[39] TLR4 is a highly conserved receptor found on macrophages, monocytes, endothelial cells, and monocyte-derived dendritic cells that recognizes pathogen-associated molecular patterns (PAMPs), such as LPS.[40−42] Moreover, low doses of LPS have been shown to enhance Th2 responses and allergic airway inflammation via TLR4 in mice after intranasal ovalbumin administration.[43] Both Der p 1 and Der p 2 have previously been reported to bind to the endocytic receptor, promoting endocytosis of the allergen.[44] TLR4 is unique among other toll-like receptors due to its ability to activate signaling from the cell−surface as well as intracellularly due to functional TRAM-TRIF signaling following endocytosis of the receptor.[45,46] This could be a potential mechanism of action, where HDM-MWCNTs are taken up by macrophages and the engulfed MWCNTs could interact with TLR4 intracellularly. LPS is a ubiquitous contaminant in many types of biomaterials and has been found to bind to the surface of nanoparticles.[47−50] Relevant to the current study, LPS is a constituent of HDM extract and therefore macrophages could interact directly with MWCNT-bound LPS via cell−surface TLR4.

Another potential mechanism through which HDM-MWCNTs could exacerbate allergic lung disease is lysosomal membrane permeabilization (LMP) after phagocytosis and compartmentalization of the HDM-MWCNTs within lysosomes. LMP is the loss of membrane integrity, which allows the release of luminal contents of the lysosome into the cytosol.[51] Lysosomes also act as signaling hubs in apoptosis and in different forms of regulated necrosis; these play a critical role in cellular responses to nanoparticles.[52,53] For example, exposure to carbon black nanoparticles induced cathepsin B-dependent pyroptosis with LMP in alveolar and RAW264.7 macrophages.[54,55] It has also been suggested that distinct cathepsins control necrotic cell death mediated by pyroptosis inducers and lysosome destabilizing agents.[56] It should be noted that the intrinsic property of the MWCNT may influence LMP. Rigidity, which is described as the ability of an MWCNT to resist deformation, may refute the idea that NC7000 MWCNTs used in the present study can elicit the same effect as long and rod-like MWCNTs on lysosomal-dependent inflammation. For example, previous studies found that long and rigid MWCNTs (NM401) triggered pyroptosis in macrophages with gasdermin D-dependent IL-1β secretion, as compared to tangled MWCNTs (NM400 and NM402) that are more similar to the tangled NC7000 MWCNTs used in the present study.[52] Similarly, it was found that while both tangled and rod-like MWCNTs both trigger acute inflammation, only rod-like MWCNTs caused frustrated phagocytosis by macrophages and chronic inflammation in mice.[57] It is argued that the strong toxicity of these rod-like MWCNTs could be due to cellular "piercing", in which MWCNT-containing phagolysosomes (i.e., frustrated phagocytosis) result in physical damage to cell membranes.[58] LMP has also been shown to trigger activation of the NLRP3 inflammasome, where the assembled inflammasome complex within the cytoplasm generates active caspase-1 to cleave pro-IL-1β and pro-IL-18 to mature forms that stimulate pyroptosis, resulting in inflammation.[59,60] Additionally, NLRP3 downregulation has also been found to inhibit phagocytosis *in vitro*.[61] However, our previous work with tangled MWCNTs suggests that the NLRP3 inflammasome and consequent IL-1β release by macrophages would not likely play a role in the exacerbation of allergic lung disease observed in the present study, since pre-exposure of mice to HDM extract suppressed MWCNT-induced IL-1β in BALF.[62] Further study is needed to determine whether HDM-MWCNTs trigger LMP more effectively than pristine MWCNTs.

Regarding allergic lung disease, it is important to make the distinction between tangled and rigid MWCNTs. The NC7000 MWCNTs used in the present study are tangled and alone did not produce an asthma-like phenotype when delivered to the lungs of mice by oropharyngeal aspiration, yet these MWCNTs strongly exacerbated allergic lung disease induced by HDM extract. This is consistent with other tangled MWCNTs that have been reported to exacerbate allergen-induced lung inflammation and fibrosis.[63] Also, as demonstrated in the present study, tangled MWCNTs produce neutrophilic inflammation in the lungs of mice yet exacerbate eosinophilic lung inflammation initiated by allergen exposure. In contrast, rigid MWCNTs (most notably Mitsui-7) produce an asthma-like phenotype in the lungs of mice, including mucous cell metaplasia, in the absence of any allergen.[57,64] However, tangled MWCNTs such as NC7000 are representative of products currently on the market that are being sold in bulk quantities, whereas rigid MWCNTs are either are being phased out due to their carcinogenic potential or are no longer in production.

Lastly, as we previously found, Der p 2 is the most abundant protein from HDM extract that was adsorbed to MWCNTs.[29] As a lipid-binding family protein,[65] Der p 2 was found to preferentially bind to cholesterol in a dose-dependent manner.[66] Lipid cargo of other lipid binding allergens, like the potential cholesterol bound to der p 2, have been found to affect allergenicity via the suppression or exacerbation of host

https://doi.org/10.1021/acsnano.4c07893
ACS Nano 2024, 18, 26215−26232

Th2 responses.[67−69] Cholesterol itself has been shown to enhance allergic responses in sensitized individuals, with increases in IgE, reduction in Th1 cytokines, and promotion of Th2 cytokine production.[70,71] It is possible that native Der p 2 could contain bound cholesterol that originates from the dietary sources of *D. pteronyssinus* or inhaled Der p 2 may interact with extracellular murine cholesterol and promote allergic responses. Further studies may provide clarity on the potential involvement of Der p 2 in the allergen corona as a lipid-binding protein that may exacerbate inhaled MWCNT responses.

An important aspect of the current study was the evaluation of potential sex differences in the exacerbation of HDM extract-induced lung disease by MWCNTs. There were no significant differences in pathological outcomes between sexes (inflammation scores, mucous cell metaplasia, airway fibrosis). However, female mice had higher numbers of total BALF cells after coexposure to HDM extract and MWCNTs or HDM-MWCNTs and this was due to higher absolute numbers of eosinophils in BALF after coexposure to MWCNTs and HDM extract or after exposure to HDM-MWCNTs. Moreover, female mice exhibited higher levels of LDH and total protein in BALF after exposure to HDM-MWCNTs but not after coexposure to HDM extract and MWCNTs. Female mice also had a significantly higher level of *Il13* mRNA compared to male mice after coexposure to HDM extract and MWCNTs, although we did not observe a significant difference in *Il13* mRNA expression between sexes after exposure to HDM-MWCNTs. IL-13 is a central mediator of allergic asthma that activates the STAT6 pathway to cause eosinophilic inflammation and mucous cell metaplasia.[72,73] Overall, the data in the present study suggests that female mice could be more susceptible than males in terms of cellular inflammatory responses to HDM extract and MWCNTs or HDM-MWCNTs. We previously reported that male C57BL6 mice, the same strain used in current study, were more susceptible to lung inflammation induced by oropharyngeal aspiration of nickel nanoparticles and LPS.[74] Others have reported that allergic airway lung inflammation was higher in female mice than male mice upon exposure to OVA sensitization and challenge, due to higher eosinophilic count, OVA-specific IgE, and production of Th2 cytokines, while having lower percentages of regulatory CD4(+)/CD25(+) T cells than males.[75] Another study concluded that airway inflammation was greater in female mice than males in response to OVA and IL-33 exposure, which is a well-known marker for a Th2 microenvironment.[76] IL-33 has been shown to amplify IL-13-induced M2a phenotype development and eotaxin 2 (CCL24) production *in vitro* and MWCNTs were demonstrated to also induce greater eosinophil recruitment in female mice upon both IL-33 and IL-13 signaling.[77−80] We did not observe any major changes in *Il33* mRNA expression in either male or female mice after coexposure to HDM extract and MWCNTs or exposure to HDM-MWCNTs in the present study.

The occupational and commercial exposures of MWCNTs have yet to be determined to exacerbate asthma in humans. While our findings do support the exacerbation of allergic lung disease in mice, a lack of epidemiological data hinder the potential reflection of these findings in real world applications. Humans are exposed to MWCNTs through inhalation and dermal exposure, and potentially through contaminated food and water.[81] It has also been reported that about 35% of patients with allergic diseases are sensitized to HDM.[82] In occupational settings, it has been reported that concentrations of 1050 $\mu g/m^3$ of MWCNTs were found during secondary manufacturing processes such as packaging and bagging of them, while also being detected in the air of manufacturing plants ranging from 0.002 to 24.9 $\mu g/m^3$.[83,84] Moreover, a cross-sectional study of 12 U.S. facilities producing carbon nanotubes and nanofibers (CNT/F) showed that 18% of participants had CNT/F in induced sputum and respiratory allergy development was positively associated with inhalable elemental carbon and number of years worked.[85] Exposure to HDM allergens can also occur in the workplace. Matuka and colleagues reported that the percentage sensitization among workers referred to the National Institute for Occupational Health (NIOH) Occupational Allergy clinic in South Africa was 41.6% for *D. farinae* and 33.8% for *D. pteronyssinus*.[86] Moreover, 19% of patients who reported work-related sickness tested positive for HDM allergens, suggesting that workplace sensitization is plausible. To our knowledge there are no reports of coexposures to MWCNTs and HDM in the workplace, although it is likely that such coexposures occur. Further epidemiological studies should provide clarity on the significance of MWCNTs in exacerbating allergic asthma in humans.

CONCLUSION

The current study explored the mechanism through which MWCNTs exacerbate HDM extract-induced allergic lung disease in mice. We discovered that the HDM-MWCNT allergen corona mediates the exacerbation of HDM-induced allergic lung disease by MWCNTs in a coexposure scenario. Our findings demonstrated that even in trace amounts, allergenic proteins from HDM extract (e.g., der p 2) adsorb on the surface of MWCNTs forming an allergen corona that amplifies biochemical, cellular and pathological aspects of allergic lung disease (STAT6 activation, induction of pro-inflammatory cytokines, eosinophilic inflammation, airway fibrosis, and mucous cell metaplasia). The increasing use of MWCNTs could increase the risk of occupational or consumer exposures, including the exacerbation of allergic asthma in environments where individuals are coexposed to nanomaterials and allergens.

MATERIALS AND METHODS

House Dust Mite Extract. HDM extract from *D. pteronyssinus* was purchased from Greer Laboratories Inc. (Lenoir, NC). Lyophilized HDM extract was dissolved in DPBS to achieve a stock total HDM extract protein concentration of 1 mg/mL, with a total yield of 4.57 mg, as measured by Bradford assay. The HDM extract [item #XPB91D3A2.5; lot #390991] contained 1610 endotoxin units, measured by amoebocyte lysate test, according to the manufacturer. Stock solution was further diluted in DPBS to achieve the necessary working concentrations for dosing.

Multiwalled Carbon Nanotubes. NC7000 MWCNTs were purchased from Nanocyl, Inc. (Sambreville, Belgium). We previously performed a thorough physicochemical characterization of these MWCNTs.[32] The physicochemical characteristics of the MWCNTs from this previous analysis are summarized in Table 1 and a TEM image is shown in Figure S1. MWCNTs were suspended in DPBS (Sigma, St. Louis, MO) to achieve a stock concentration of 3.3 mg/mL. Prepared stock of MWCNTs suspension was sonicated in a cup horn sonicator (Q500, Qsonica, Newtown, CT) for 10 min at 60 A. Stock solution was further diluted with DPBS to achieve the necessary working conditions for dosing. The dosing strategy for delivering MWCNTs to the lungs of mice by oropharyngeal aspiration in the absence or presence of HDM extract is illustrated in Figure 1.

https://doi.org/10.1021/acsnano.4c07893
ACS Nano 2024, 18, 26215−26232

Dynamic light scattering (DLS; Zetasizer, Malvern Instruments, Worcestershire, England) was used to measure the hydrodynamic diameter and polydispersity index of MWCNTs (500 mg/mL in 0.01X PBS in water) and HDM-MWCNT protein coronas (500 mg/mL of HDM incubated with 500 mg/mL MWCNT in 0.01X PBS in water). Measurements were carried out in triplicate with three distinct samples. Average and standard deviation are reported for all measurements. The DLS results are shown in Figure S3.

Preparation and Characterization of HDM-MWCNT Allergen Corona Samples. Concentrations of 10 μg/mL MWCNTs and 1.84 μg/mL HDM extract were incubated in DPBS on an Aliquot Mixer (Ames model #4651) in 10 mL collection tubes for 30 min. Following rocking, samples were vortexed for 10 s at highest speed and centrifuged at 12,000 rpm for 20 min. Supernatant was replaced with equal volume of DPBS. The pellets were vortexed for 10 s at highest speed and centrifuged at 12,000 rpm for 20 min. The cycle was completed for a total of 3 times. The pristine MWCNTs used as a comparison to the HDM-MWCNTs went through the same washing and resuspension protocol after centrifugation. The final samples were resuspended in 50 μL of DPBS for dosing mice. We previously conducted a thorough proteomic analysis of the HDM-MWCNT corona proteins using liquid chromatography with tandem mass spectrometry (LC−MS/MS) to identify proteins in HDM extract and the HDM corona formed on MWCNTs (HDM-MWCNTs).[29] Moreover, the same lot of HDM extract that was used in our previous proteomic analysis was used in the present study. The normalized abundance (% of total protein) of top 10 proteins in HDM extract and in the HDM-MWCNT corona from this analysis are shown in Figure 5B.

Analysis of Total Protein and der p Allergens in HDM-MWCNT Coronas. HDM-MWCNTs were prepared as described above, with concentrations of 1.84 μg/mL of HDM extract and 10 μg/mL of MWCNTs. After the final centrifugation step, samples were resuspended in 1 mL of lysis buffer (20 mM Tris−HCl, 150 mM NaCl, 1 mM EDTA, 1 mM EGTA, 1% triton X-100, 1 mM Na_3VO_4, 1× halt protease inhibitor cocktail, in DPBS). The resulting mixture was centrifuged at 2000 rpm for 5 min. The resulting supernatant was removed from the pelleted MWCNTs. 1.84 μg/mL of HDM extract was diluted in lysis buffer for HDM-alone positive control. The protein concentration of the supernatant and HDM positive control was determined using the Pierce BCA Protein Assay Kit (ThermoFisher Scientific, Waltham, MA). Absorbance was read at 450 nm with a correction at 540 nm using the Multiskan EX microplate spectrophotometer (ThermoFisher, Waltham, MA). Samples were loaded onto a Criterion TGX stain-free precast 4−15% SDS-PAGE gel (Bio-Rad Laboratories Inc., Hercules, CA), and separated by electrophoresis and transferred onto PVDF membranes. Membranes were blocked for 1 h and incubated overnight in 1:1000 dilution of primary antibodies purchased from RayBiotech (Norcross, GA) der P1, #130-10,020 and antibodies-online.com (Limerick, PA) (der P2, #ABIN7141165). Following primary antibody incubation, transferred membranes were washed and incubated in 1:2500 dilution (Cell Signaling Technology, Danvers, MA) with horseradish peroxidase-conjugated secondary antirabbit antibody. Enhanced chemiluminescence (ECL) Prime Western Blotting Detection Reagent (Cytiva, Marlborough, MA) was used to facilitate HRP-induced chemiluminescence according to the manufacturer's instructions. Resulting signals were captured using Amersham Imager 680 (GE Life Sciences, Marlborough, MA) and semiquantitative densitometry was performed using ImageQuant software (GE Life Sciences, Marlborough, MA).

Animal Care. Wildtype (WT) male and female C57BL/6J mice (8-10 weeks) were purchased from The Jackson Laboratory (Bar Harbor, ME). Mice were housed in an AAALAC (association for assessment and accreditation of Laboratory Animal Care) accredited animal facility, which was humidity/temperature controlled, pathogen-free, and supplied with food and water ad libitum. All animal procedures were approved by the NC State University Institutional Animal Care and Committee (IACUC). Mice were housed 5 per cage according to their respective treatment groups and sex—vehicle control, MWCNTs, HDM extract, MWCNTs + HDM extract, and MWCNT-HDM allergen corona.

Exposure of Mice to MWCNTs and HDM Extract. Mice were exposed by oropharyngeal aspiration (OPA) to 50 μL of the following treatments: vehicle solution control, MWCNTs, HDM extract, both, or by MWCNT-HDM allergen corona. Dosing strategy included exposure strategies in both the sensitization phase (days 1, 3, and 5) and the challenge phase (days 15, 17, and 19). All treatments were prepared in a DPBS (Sigma) vehicle solution and were vortexed immediately before delivery to mice by oropharyngeal aspiration (OPA) under isoflurane anesthesia. For the first experiment using MWCNTs in the presence or absence of HDM extract, male and female WT mice were exposed to vehicle or 0.02 mg/kg body weight of HDM per dosing session (0.4 μg/female mouse; 0.5 μg/male mouse) with or without 0.5 mg/kg body weight of MWCNTs (10 μg/female mouse; 12.5 μg/male mouse). In the second experiment introducing the MWCNT-HDM allergen corona, male and female WT mice were exposed to vehicle or 0.5 mg/kg body weight (10 μg/female mouse; 12.5 μg/male mouse) MWCNTs with or without 0.092 mg/kg body weight (1.84 μg/female mouse; 2.3 μg/male mouse) of HDM extract per dosing session.

Necropsy and Sample Collection. Necropsy was performed on day 22 following euthanization with an intraperitoneal injection of pentobarbital. Bronchoalveolar lavage fluid (BALF) was collected from each mouse by cannulating the trachea and conducting lavages of the lungs with 0.5 mL of chilled DPBS two times. 100 μL of the BALF was collected for differential cell counts and 10 μL was collected for total BALF cell counts. The remaining BALF was centrifuged at 2000 rpm for 5 min and the resulting supernatant was transferred to a separate set of tubes and utilized for analysis of protein, LDH, and cytokines/chemokines. The cell pellet was resuspended in 200 μL DPBS and used to analyze inflammatory cells. For histopathology, the left lung lobe was fixed in neutral buffered formalin (VWR, Radnor, PA) for 24 h, then transferred to 70% ethanol for a week before being embedded in paraffin. For mRNA analysis, a right superior lung lobe was stored in RNAlater (Fisher Scientific, Waltham, MA) and stored at −80 °C. For protein analysis, the right medial and inferior lung lobes were snap frozen in liquid nitrogen and stored at −80 °C.

BALF Inflammatory Cell Counts. Total BALF cell counts were performed using a hemocytometer. For differential cell counts, 100 μL of BALF was centrifuged onto glass slides using a Cytospin 4 centrifuge (ThermoFisher, Waltham, MA) and the slides were then fixed and stained with the Diff-Quik stain set (Epredia, Kalamazoo, MI). Cell differentials were quantified by counting up to 500 cells per slide using an Olympus light microscope BX41 (Center Valley, PA) to determine relative numbers of macrophages, neutrophils, eosinophils, and lymphocytes. Data was presented as a proportion of total cells on slide.

Cytokine Analysis in BALF. DuoSet enzyme-linked immunosorbent assay (ELISA) kits (R&D Systems, Minneapolis, MN) were used according to the manufacturer's protocol to quantify protein levels of cytokines C-X-C motif chemokine ligand 2 (CXCL2), interleukin 1 beta (IL-1β), interleukin 33 (IL-33), and tumor necrosis factor alpha (TNF-α) from BALF. Concentrations of cytokines were resulting from the absorbance values measured at 450 nm with a background correction at 540 nm using the Multiskan EX microplate spectrophotometer (ThermoFisher, Waltham, MA). Standard curves were used to derive cytokine concentrations based on the manufacturer's protocol (GraphPad Prism, version 10.0, La Jolla, CA).

Cytotoxicity and Total Protein in BALF. LDH activity in BALF was assayed as an indicator for pulmonary cytotoxicity with the "pierce LDH Cytotoxicity Assay Kit" (ThermoFisher, Waltham, MA), according to the manufacturer's instructions. Absorbance values were measured at 450 nm using a Multiskan EX microplate spectrophotometer (ThermoFisher). Total protein concentration in BALF was determined using the "Pierce BCA Protein Assay Kit" (ThermoFisher), according to the manufacturer's instructions.

https://doi.org/10.1021/acsnano.4c07893
ACS Nano 2024, 18, 26215−26232

qRT-PCR. The right superior lungs were frozen and stored in RNAlater (Fisher Scientific, Waltham, MA). Frozen lung samples were thawed to 4 °C. Thawed lung samples were moved to 1.5 mL centrifugation tubes containing RNA lysis buffer (Zymo Research, Irvine, CA). Two 35 mm stainless steel beads were inserted into each 1.5 mL collection tube containing lung sample and RNA lysis buffer to facilitate tissue homogenization. Mini Bead Mill Homogenizer (VWR International) was used with a speed setting of 4 for 1 min. The resulting mixture was centrifuged at 5000 rpm for 5 min. Applied Biosystems high-capacity cDNA reverse transcription kit (ThermoFisher Scientific, Waltham, MA) was used to create cDNA from the mRNA isolated from the right lung lobe using Quick-RNA MiniPrep (Zymo Research, Irvine, CA) according to the manufacturer's instructions. The FastStart Universal Probe Master (Rox) (Roche, Basel, Switzerland) was used to run Taqman qPCR on the Applied Biosystems QuantStudio3 Real-Time PCR System Thermal Cycling Block (ABI, Foster City, CA) to determine the comparative C_T ($\Delta\Delta C_T$) fold change expression of specific mRNAs (*Col1a1*, *Arg1*, *IL-6*, *Ccl-11*) normalized to *B2M* as the endogenous control.

Immunoblotting. Snap-frozen right lung lobe samples were transferred to 1.5 mL centrifugation tubes containing lysis buffer (20 mM Tris−HCl, 150 mM NaCl, 1 mM EDTA, 1 mM EGTA, 1% triton X-100, 1 mM Na_3VO_4, 1 × halt protease inhibitor cocktail, in DPBS). Two 35 mm stainless steel beads were inserted into each 1.5 mL centrifugation tube containing right lung sample and lysis buffer to assist tissue homogenization. Mini Bead Mill Homogenizer (VWR International) was used with a speed setting of 4 for 1 min. The resulting lysate was spun down at 2000 rpm for 5 min. The protein concentration of the supernatant was determined using the Pierce BCA Protein Assay Kit (ThermoFisher Scientific, Waltham, MA). Absorbance was read at 450 nm with a correction at 540 nm using the Multiskan EX microplate spectrophotometer (ThermoFisher, Waltham, MA). Samples were loaded onto a Criterion TGX stain-free precast 4−15% SDS-PAGE gel (Bio-Rad Laboratories Inc., Hercules, CA), and separated by electrophoresis and transferred onto PVDF membranes. Membranes were blocked for 1 h and incubated overnight in 1:1000 dilution of rabbit or mouse primary antibodies purchased from Cell Signaling Technology (phosphorylated STAT6 at Tyr640, #56554S; STAT6, #5397S; and β-actin, #4967L). Following primary antibody incubation, transferred membranes were washed and incubated in 1:2500 dilution (Cell Signaling Technology, Danvers, MA) with horseradish peroxidase-conjugated secondary antirabbit antibody. Enhanced chemiluminescence (ECL) Prime Western Blotting Detection Reagent (Cytiva, Marlborough, MA) was used to facilitate HRP-induced chemiluminescence according to the manufacturer's instructions. Resulting signals were captured using Amersham Imager 680 (GE Life Sciences, Marlborough, MA) and semiquantitative densitometry was performed using ImageQuant software (GE Life Sciences, Marlborough, MA).

Histopathology. The left lung was cut into three cross sections, which were embedded in paraffin, and 5 μm histologic sections were mounted on charged glass slides. Sections were stained with the following: Hematoxylin and eosin (H&E) to assess pro-inflammatory tissue reactions, Masson's trichrome for collagen deposition, and Alcian blue/periodic acid-Schiff (AB/PAS) for mucus production.

Quantitative Scoring of Airway Inflammation. Microscope slides with lung tissue sections stained with hematoxylin and eosin were evaluated for inflammation using a 4× objective (inflammatory cells and thickness of the alveolar walls). Inflammation scores were assigned by three independent observers using the following scale: 1 - normal lung tissue as seen in the WT control group, 2 - minimal change, 3 - mild change, 4 - moderate change, and 5 - marked change. Data were presented as the mean ± SEM of the inflammation score for each dose group in both genotypes.

Quantitative Morphometry of Airway Fibrosis and Mucous Cell Metaplasia. Airway fibrosis, based on Gomori's trichrome-stained slides, was assessed by measuring thickness of the collagen layer, surrounding the airways, using an area/perimeter ratio method, as described previously.[8,74,75] Approximately 10 airways per lung cross sections per mouse (3 cross sections per mouse, resulting in a total of 30 photomicrographs per mouse) that fit to our criteria (circular airways that fit in the field of view) were photographed at 100× magnification using an Olympus BX41 light microscope (Center Valley, PA). To determine the area/perimeter ratio, round to oval shaped airways under 500 × 500 μm (H × W) were imaged at 100 ×. The lasso tool in Adobe Photoshop CS5 was used to surround trichrome positive collagen around the airways, giving the outer area, and to surround the basement membrane, giving the inner area and circumference (perimeter). The difference between the outer and inner area was divided by the circumference giving the area/perimeter ratio. All measurements were performed in a blinded manner. Mucous cell metaplasia and airway mucus production assessed by imaging all airways under approximately 500 × 500 μm (H × W) in each AB/PAS-stained sample and quantifying the area of positive staining in ImageJ (National Institutes of Health) as a percent area.

Statistical Analysis. One-way ANOVA with Tukey's post hoc test or Student's *t*-test was used to evaluate differences between treatment groups (GraphPad Prism, version 10.0, La Jolla, CA). Two-way ANOVA with a Tukey's post hoc test was utilized to evaluate differences among treatment and sex groups. All data represent the mean ± SEM of five animal replicates.

ASSOCIATED CONTENT

Data Availability Statement

Data sets generated for this study are available from the corresponding author upon reasonable request.

Supporting Information

The Supporting Information is available free of charge at https://pubs.acs.org/doi/10.1021/acsnano.4c07893.

> Absolute numbers of macrophages, eosinophils, and neutrophils in each treatment group from which the percentage of each cell type was derived shown in Figure 1 (Figure S1); original Western blot images used in Figure 4 (Figure S2); DLS results showing the hydrodynamic diameter and polydispersity index (PDI) of pristine MWCNTs and MWCNTs with HDM allergen corona (HDM-MWCNT) (Figure S3). Absolute numbers of macrophages, eosinophils, and neutrophils in each treatment group from which the percentage of each cell type was derived shown in Figure 7 (Figure S4). Original Western blot images used in Figure 9 (Figure S5) (PDF)

AUTHOR INFORMATION

Corresponding Author

James C. Bonner − *Toxicology Program, Department of Biological Sciences, North Carolina State University, Raleigh, North Carolina 27695, United States;* orcid.org/0000-0002-4574-9782; Email: jcbonner@ncsu.edu

Authors

Ryan D. Bartone − *Toxicology Program, Department of Biological Sciences, North Carolina State University, Raleigh, North Carolina 27695, United States*

Logan J. Tisch − *Toxicology Program, Department of Biological Sciences, North Carolina State University, Raleigh, North Carolina 27695, United States*

Judith Dominguez − *Thomas Lord Department of Mechanical Engineering and Materials Science, Duke University, Durham, North Carolina 27708, United States*

Christine K. Payne − *Thomas Lord Department of Mechanical Engineering and Materials Science, Duke University, Durham, North Carolina 27708, United States;* orcid.org/0000-0002-2370-0101

https://doi.org/10.1021/acsnano.4c07893
ACS Nano 2024, 18, 26215−26232

Complete contact information is available at:
https://pubs.acs.org/10.1021/acsnano.4c07893

Author Contributions

RDB, LJT, JD, CKP and JCB designed the experiments and participated in data interpretation. RDB, LJT, JD, and JCB performed the experiments and data analysis. RDB and JCB wrote the manuscript. All other coauthors edited the manuscript.

Funding

This work was funded by National Institute of Environmental Health Sciences (NIEHS) grant R01ES032443 and NIEHS grant P30ES025128. RDB and LJT were partially supported by NIEHS Training Grant T32ES007046. JD was partially supported by the National Science Foundation Graduate Research Fellowship under DGE 2139754.

Notes

Ethics approval: The animal study was approved by the North Carolina State University Animal. Care and Use Committee (NCSU IACUC protocol #19-681).
The authors declare no competing financial interest.

ABBREVIATIONS

MWCNT	multiwalled carbon nanotubes
HDM	house dust mite
HDM-MWCNT	MWCNTs with HDM corona
BALF	bronchoalveolar lavage fluid
LDH	lactate dehydrogenase
ENM	engineered nanomaterial
CCL11	eotaxin-1
IL-6	interleukin-6
ARG-1	arginase-1
NFκB	nuclear factor κB
OPA	oropharyngeal aspiration
STAT-6	signal transducer and activator of transcription 6
TLR4	toll-like receptor 4

REFERENCES

(1) Iijima, S. Helical Microtubules of Graphitic Carbon. *Nature* **1991**, *354*, 56−58.
(2) Jensen, K. A.; Bøgelund, J.; Jackson, P.; Jacobsen, N. R.; Birkedahl, R.; Clausen, P. A.; Saber, A. T.; Wallin, H.; Vogel, U. B. Carbon Nanotubes—Types, Products, Market, and Provisional Assessment of the Associated Risks to Man and the Environment. *Ministry of Environment and Food of Denmark* 2015.
(3) Bianco, A.; Kostarelos, K.; Prato, M. Applications of Carbon Nanotubes in Drug Delivery. *Curr. Opin. Chem. Biol.* **2005**, *9*, 674−679.
(4) Carvalho, S.; Ferrini, M.; Herritt, L.; Holian, A.; Jaffar, Z.; Roberts, K. Multi-Walled Carbon Nanotubes Augment Allergic Airway Eosinophilic Inflammation by Promoting Cysteinyl Leukotriene Production. *Front. Pharmacol* **2018**, *9*, 585.
(5) Czarny, B.; Georgin, D.; Berthon, F.; Plastow, G.; Pinault, M.; Patriarche, G.; Thuleau, A.; L'Hermite, M. M.; Taran, F.; Dive, V. Carbon Nanotube Translocation to Distant Organs after Pulmonary Exposure: Insights from *in Situ* ^{14}C-Radiolabeling and Tissue Radioimaging. *ACS Nano* **2014**, *8*, 5715−5724.
(6) Ryman-Rasmussen, J. P.; Cesta, M. F.; Brody, A. R.; Shipley-Phillips, J. K.; Everitt, J. I.; Tewksbury, E. W.; Moss, O. R.; Wong, B. A.; Dodd, D. E.; Andersen, M. E.; Bonner, J. C. Inhaled Carbon Nanotubes Reach the Subpleural Tissue in Mice. *Nat. Nanotechnol.* **2009**, *4*, 747−751.
(7) Ryman-Rasmussen, J. P.; Tewksbury, E. W.; Moss, O. R.; Cesta, M. F.; Wong, B. A.; Bonner, J. C. Inhaled Multiwalled Carbon Nanotubes Potentiate Airway Fibrosis in Murine Allergic Asthma. *Am. J. Respir. Cell Mol. Biol.* **2009**, *40*, 349−358.
(8) Lee, H. Y.; You, D. J.; Taylor-Just, A. J.; Tisch, L. J.; Bartone, R. D.; Atkins, H. M.; Ralph, L. M.; Antoniak, S.; Bonner, J. C. Role of the Protease Activated Receptor-2 (PAR2) in the Exacerbation of House Dust Mite-Induced Murine Allergic Lung Disease by Multi-Walled Carbon Nanotubes. *Part. Fibre Toxicol.* **2023**, *20*, 32.
(9) Holgate, S. T. Pathogenesis of Asthma. In *Allergy and Allergic Diseases*; Kay, A. B., Kaplan, A. P., Bousquet, J., Holt, P. G., Eds.; Wiley-Blackwell: NJ, 2008; pp 1608−1631.
(10) Braman, S. S. The Global Burden of Asthma. *Chest* **2006**, *130*, 4S−12S.
(11) Kim, H. Y.; DeKruyff, R. H.; Umetsu, D. T. The Many Paths to Asthma: Phenotype Shaped by Innate and Adaptive Immunity. *Nat. Immunol.* **2010**, *11*, 577−584.
(12) Finkelman, F. Cytokine Regulation of Type 2 Immunity. In *Samter's Immunologic Diseases*, 6 ed.; Austen, K. F., Frank, M. M., Atkinson, J. P., Cantor, H., Eds.; Lippincott Williams & Wilkins: Philadelphia, 2001; pp 111−126. th Ed..
(13) Hamid, Q.; Tulic, M. Immunobiology of Asthma. *Annu. Rev. Physiol.* **2009**, *71*, 489−507.
(14) Reid, C. E.; Brauer, M.; Johnston, F. H.; Jerrett, M.; Balmes, J. R.; Elliott, C. T. Critical Review of Health Impacts of Wildfire Smoke Exposure. *Environ. Health Perspect.* **2016**, *124*, 1334−1343.
(15) Riedl, M. A.; Diaz-Sanchez, D.; Liinn, W. S.; Gong, H., Jr; Clark, K. W.; Effros, R. M.; Miller, J. W.; Cocker, D. R.; Berhane, K. T.; H.E.I. Health Review Committee. Allergic Inflammation in the Human Lower Respiratory Tract Affected by Exposure to Diesel Exhaust. *Res. Rep. − Health Eff. Inst.* **2012**, *165*, 5−43.
(16) Ihrie, M. D.; Bonner, J. C. The Toxicology of Engineered Nanomaterials in Asthma. *Curr. Environ. Health Rep.* **2018**, *5*, 100−109.
(17) Utembe, W.; Andraos, C.; Gulumian, M. Immunotoxicity of Engineered Nanomaterials and Their Role in Asthma. *Crit. Rev. Toxicol.* **2023**, *53*, 491−505.
(18) Runa, S.; Hussey, M.; Payne, C. K. Nanoparticle-Cell Interactions: Relevance for Public Health. *J. Phys. Chem. B* **2018**, *122*, 1009−1016.
(19) Mahmoudi, M.; Landry, M. P.; Moore, A.; Coreas, R. The Protein Corona from Nanomedicine to Environmental Science. *Nat. Rev. Mater.* **2023**, *8*, 422−438.
(20) Kobos, L.; Shannahan, J. Biocorona-Induced Modifications in Engineered Nanomaterial-Cellular Interactions Impacting Biomedical Applications. *Wiley Interdiscip. Rev.: Nanomed. Nanobiotechnol.* **2020**, *12*, No. e1608.
(21) Lynch, I.; Cedervall, T.; Lundqvist, M.; Cabaleiro-Lago, C.; Linse, S.; Dawson, K. A. The Nanoparticle-Protein Complex as a Biological Entity; a Complex Fluids and Surface Science Challenge for the 21st Century. *Adv. Colloid Interface Sci.* **2007**, *134*−*135*, 167−174.
(22) Monopoli, M. P.; Åberg, C.; Salvati, A.; Dawson, K. A. Biomolecular Coronas Provide the Biological Identity of Nanosized Materials. *Nat. Nanotechnol.* **2012**, *7*, 779−786.
(23) Ke, P. C.; Lin, S.; Parak, W. J.; Davis, T. P.; Caruso, F. A Decade of the Protein Corona. *ACS Nano* **2017**, *11*, 11773−11776.
(24) Nel, A. E.; Mädler, L.; Velegol, D.; Xia, T.; Hoek, E. M. V.; Somasundaran, P.; Klaessig, F.; Castranova, V.; Thompson, M. Understanding Biophysicochemical Interactions at the Nano-Bio Interface. *Nat. Mater.* **2009**, *8*, 543−557.
(25) Lynch, I.; Dawson, K. A. Protein-Nanoparticle Interactions. *Nano. Today.* **2008**, *3*, 40−47.
(26) Zhao, X.; Liu, R.; Chi, Z.; Teng, Y.; Qin, P. New Insights into the Behavior of Bovine Serum Albumin Adsorbed Onto Carbon Nanotubes: Comprehensive Spectroscopic Studies. *J. Phys. Chem. B* **2010**, *114*, 5625−5631.
(27) Bai, W.; Wu, Z.; Mitra, S.; Brown, J. M. Effects of Multiwalled Carbon Nanotube Surface Modification and Purification on Bovine Serum Albumin Binding and Biological Responses. *J. Nanomater.* **2016**, *2016*, 1−10.

(28) Radauer-Preiml, I.; Andosch, A.; Hawranek, T.; Luetz-Meindl, U.; Wiederstein, M.; Horejs-Hoeck, J.; Himly, M.; Boyles, M.; Duschl, A. Nanoparticle-Allergen Interactions Mediate Human Allergic Responses: Protein Corona Characterization and Cellular Responses. *Part. Fibre Toxicol.* **2015**, *13*, 3.
(29) Dominguez, J.; Holmes, S. K.; Bartone, R. D.; Tisch, L. J.; Tighe, R. M.; Bonner, J. C.; Payne, C. K. House Dust Mite Extract Forms a Der p 2 Corona on Multi-Walled Carbon Nanotubes: Implications for Allergic Airway Disease. *Environ. Sci.: Nano* **2024**, *11*, 324−335.
(30) Gomez, S.; Gamazo, C.; San Roman, B.; Grau, A.; Espuelas, S.; Ferrer, M.; Sanz, M. L.; Irache, J. M. A novel Nanoparticulate Adjuvant for Immunotherapy with *Lolium perenne*. *J. Immunol. Methods* **2009**, *348*, 1−8.
(31) Licciardi, M.; Montana, G.; Bondi, M. L.; Bonura, A.; Scialabba, C.; Melis, M.; Fiorica, C.; Giammona, G.; Colombo, P. An Allergen-polymeric Nanoaggregate as a New Tool for Allergy Vaccination. *Pharm. Nanotechnol.* **2014**, *465*, 275−283.
(32) Taylor-Just, A. J.; Ihrie, M. D.; Duke, K. S.; Lee, H. Y.; You, D. J.; Hussain, S.; Kodali, V. K.; Ziemann, C.; Creutzenberg, O.; Vulpoi, A.; Turcu, F.; Potara, M.; Todea, M.; van den Brule, S.; Lison, D.; Bonner, J. C. The Pulmonary Toxicity of Carboxylated or Aminated Multi-Walled Carbon Nanotubes in Mice is Determined by the Prior Purification Method. *Part. Fibre Toxicol.* **2020**, *17*, 60.
(33) Chapman, M. D.; Platts-Mills, T. Purification and Characterization of the Major Allergen from *Dermatophagoides Pteronyssinus*-Antigen P1. *J. Immunol.* **1980**, *125*, 587−592.
(34) Ye, Y.-L.; Wu, H.-T.; Lin, C.-F.; Hsieh, C.-Y.; Wang, J.-Y.; Liu, F.-H.; Ma, C. T.; Bei, C.-H.; Cheng, Y.-L.; Chen, C.-C.; Chiang, B.-L.; Tsao, C.-W. *Dermatophagoides pteronyssinus* 2 Regulates Nerve Growth Factor Release to Induce Airway Inflammation *via* Reactive Oxygen Species-Dependent Pathway. *Am. J. Physiol. Lung Cell. Mol. Physiol.* **2011**, *300* (2), L216−L224.
(35) Klein, M.; Colas, L.; Cheminant, M.-A.; Brosseau, C.; Sauzeau, V.; Magnan, A.; Bouchaud, G. Der p 2.1 Peptide Abrogates House Dust Mites-Induced Asthma Features in Mice and Humanized Mice by Inhibiting DC-Mediated T Cell Polarization. *Front. Immunol.* **2020**, *11*, 565431.
(36) Zhang, T.; Tang, M.; Yao, Y.; Ma, Y.; Pu, Y. MWCNT Interactions with Protein: Surface-Induced Changes in Protein Adsorption and the Impact of Protein Corona on Cellular Uptake and Cytotoxicity. *Int. J. Nanomedicine.* **2019**, *14*, 993−1009.
(37) Reginald, K.; Chew, F. T. The Major Allergen Der p 2 is a Cholesterol Binding Protein. *Sci. Reports.* **2019**, *9*, 1556.
(38) Cyphert-Daly, J. M.; Yang, Z.; Ingram, J. L.; Tighe, R. M.; Que, L. G. Physiologic Response to Chronic House Dust Mite Exposure in Mice is Dependent on Lot Characteristics. *J. Allergy Clin. Immunol.* **2019**, *144*, 1428−1432.e8.
(39) Trompette, A.; Divanovic, S.; Visintin, A.; Blanchard, C.; Hegde, R. S.; Madan, R.; Thorne, P. S.; Wills-Karp, M.; Gioannini, T. L.; Weiss, J. P.; Karp, C. L. Allergenicity Resulting from Functional Mimicry of a Toll-Like Receptor Complex Protein. *Nature* **2009**, *457*, 585−588.
(40) Akira, S.; Takeda, K. Toll-like receptor signalling. *Nat. Rev. Immunol.* **2004**, *4*, 499−511.
(41) Blecher-Gonen, R.; Bost, P.; Hilligan, K. L.; David, E.; Salame, T. M.; Roussel, E.; Connor, L. M.; Mayer, J. U.; Bahar Halpern, K.; Tóth, B.; Itzkovitz, S.; Schwikowski, B.; Ronchese, F.; Amit, I. Single-Cell Analysis of Diverse Pathogen Responses Defines a Molecular Roadmap for Generating Antigen-Specific Immunity. *Cell Syst.* **2019**, *8*, 109−121.e6.
(42) Miller, J. C.; Brown, B. D.; Shay, T.; Gautier, E. L.; Jojic, V.; Cohain, A.; Pandey, G.; Leboeuf, M.; Elpek, K. G.; Helft, J.; Hashimoto, D.; Chow, A.; Price, J.; Greter, M.; Bogunovic, M.; Bellemare-Pelletier, A.; Frenette, P. S.; Randolph, G. J.; Turley, S. J.; Merad, M.; et al. Deciphering the Transcriptional Network of the Dendritic Cell Lineage. *Nat. Immunol.* **2012**, *13*, 888−899.
(43) Eisenbarth, S. C.; Piggott, D. A.; Huleatt, J. W.; Visintin, I.; Herrick, C. A.; Bottomly, K. Lipopolysaccharide-Enhanced, Toll-Like Receptor 4-Dependent T Helper Cell Type 2 Responses to Inhaled Antigen. *J. Exp. Med.* **2002**, *196*, 1645−1651.
(44) Royer, P. J.; Emara, M.; Yang, C.; Al-Ghouleh, A.; Tighe, P.; Jones, N.; Sewell, H. F.; Shakib, F.; Martinez-Pomares, L.; Ghaemmaghami, A. M. The Mannose Receptor Mediates the Uptake of Diverse Native Allergens by Dendritic Cells and Determines Allergen-Induced T Cell Polarization Through Modulation of IDO Activity. *J. Immunol.* **2010**, *185*, 1522−1531.
(45) Kagan, J. C.; Su, T.; Horng, T.; Chow, A.; Akira, S.; Medzhitov, R. TRAM couples endocytosis of Toll-like receptor 4 to the induction of interferon-β. *Nat. Immunol.* **2008**, *9*, 361−368.
(46) Husebye, H.; Halaas, Ø.; Stenmark, H.; Tunheim, G.; Sandanger, Ø.; Bogen, B.; Brech, A.; Latz, E.; Espevik, T. Endocytic Pathways Regulate Toll-Like Receptor 4 Signaling and Link Innate and Adaptive Immunity. *EMBO J.* **2006**, *25*, 683−692.
(47) Gorbet, M. B.; Sefton, M. V. Endotoxin: The Uninvited Guest. *Biomaterials* **2005**, *26*, 6811−6817.
(48) Li, Y.; Boraschi, D. Endotoxin Contamination: A Key Element in the Interpretation of Nanosafety Studies. *Nanomedicine* **2016**, *11*, 269−287.
(49) Darkow, R.; Groth, T.; Albrecht, W.; Lützow, K.; Paul, D. Functionalized Nanoparticles for Endotoxin Binding in Aqueous Solutions. *Biomaterials* **1999**, *20*, 1277−1283.
(50) Li, Y.; Shi, Z.; Radauer-Preiml, I.; Andosch, A.; Casals, E.; Luetz-Meindl, U.; Cobaleda, M.; Lin, Z.; Jaberi-Douraki, M.; Italiani, P.; Horejs-Hoeck, J.; Himly, M.; Monteiro-Riviere, N. A.; Duschl, A.; Puntes, V. F.; Boraschi, D. Bacterial Endotoxin (Lipopolysaccharide) Binds to the Surface of Gold Nanoparticles, Interferes with Biocorona Formation and Induces Human Monocyte Inflammatory Activation. *Nanotoxicology* **2017**, *11*, 1157−1175.
(51) Wang, F.; Gómez-Sintes, R.; Boya, P. Lysosomal Membrane Permeabilization and Cell Death. *Traffic* **2018**, *19*, 918−931.
(52) Keshavan, S.; Gupta, G.; Martin, S.; Fadeel, B. Multi-Walled Carbon Nanotubes Trigger Lysosome-Dependent Cell Death (Pyroptosis) in Macrophages but not in Neutrophils. *Nanotoxicology* **2021**, *15*, 1125−1150.
(53) Andón, F. T.; Fadeel, B. Programmed Cell Death: Molecular Mechanisms and Implications for Safety Assessment of Nanomaterials. *Acc. Chem. Res.* **2013**, *46*, 733−742.
(54) Yuan, X.; Nie, W.; He, Z.; Yang, J.; Shao, B.; Ma, X.; Zhang, X.; Bi, Z.; Sun, L.; Liang, X.; Tie, Y.; Liu, Y.; Mo, F.; Xie, D..; Wei, Y.; Wei, X. Carbon Black Nanoparticles Induce Cell Necrosis through Lysosomal Membrane Permeabilization and Cause Subsequent Inflammatory Response. *Theranostics* **2020**, *10*, 4589−4605.
(55) Reisetter, A. C.; Stebounova, L. V.; Baltrusaitis, J.; Powers, L.; Gupta, A.; Grassian, V. H.; Monick, M. M. Induction of Inflammasome-Dependent Pyroptosis by Carbon Black Nanoparticles. *J. Biol. Chem.* **2011**, *286*, 21844−21852.
(56) Brojatsch, J.; Lima, H.; Palliser, D.; Jacobson, L. S.; Muehlbauer, S. M.; Furtado, R.; Goldman, D. L.; Lisanti, M. P.; Chandran, K. Distinct Cathepsins Control Necrotic Cell Death Mediated by Pyroptosis Inducers and Lysosome-Destabilizing Agents. *Cell Cycle* **2015**, *14*, 964−972.
(57) Duke, K. S.; Taylor-Just, A. J.; Ihrie, M. D.; Shipkowski, K. A.; Thompson, E. A.; Dandley, E. C.; Parsons, G. N.; Bonner, J. C. STAT1-Dependent and -Independent Pulmonary Allergic and Fibrogenic Responses in Mice After Exposure to Tangled Versus Rod-like Multi-Walled Carbon Nanotubes. *Part. Fibre Toxicol.* **2017**, *14*, 26.
(58) Westphal, G. A.; Rosenkranz, N.; Brik, A.; Weber, D.; Föhring, I.; Monsé, C.; Kaiser, N.; Hellack, B.; Mattenklott, M.; Brüning, T.; Johnen, G.; Bünger, J. Multi-Walled Carbon Nanotubes Induce Stronger Migration of Inflammatory Cells In Vitro than Asbestos or Granular Particles but a Similar Pattern of Inflammatory Mediators. *Toxicol. In Vitro* **2019**, *58*, 215−223.
(59) de Zoete, M. R.; Palm, N. W.; Zhu, S.; Flavell, R. A. Inflammasomes. *Cold Spring Harbor Perspect. Biol.* **2014**, *6*, a016287.
(60) Latz, E.; Xiao, T. S.; Stutz, A. Activation and Regulation of the Inflammasomes. *Nat. Rev. Immunol.* **2013**, *13*, 397−411.

https://doi.org/10.1021/acsnano.4c07893
ACS Nano 2024, 18, 26215−26232

(61) Li, Q.; Zhao, F.; Zhang, J.; Yang, Y.; Guo, Z.; Wang, C.; Yang, Q.; Sun, Y.; Zhu, Z. NLRP3 Inflammasome Simultaneously Involved in Autophagy and Phagocytosis of THP-1 Cells to Clear Aged Erythrocytes. *J. Immunol. Res.* **2022**, *2022*, 1−24.
(62) Shipkowski, K. A.; Taylor, A. J.; Thompson, E. A.; Glista-Baker, E. E.; Sayers, B. C.; Messenger, Z. J.; Bauer, R. N.; Jaspers, I.; Bonner, J. C. An Allergic Lung Microenvironment Suppresses Carbon Nanotube-Induced Inflammasome Activation Via STAT6-Dependent Inhibition of Caspase-1. *PLoS One* **2015**, *10*, No. e0128888.
(63) Ihrie, M. D.; Duke, K. S.; Shipkowski, K. A.; You, D. J.; Lee, H. Y.; Taylor-Just, A. J.; Bonner, J. C. STAT6-Dependent Exacerbation of House Dust Mite-Induced Allergic Airway Disease in Mice by Multi-Walled Carbon Nanotubes. *NanoImpact.* **2021**, *22*, 100309.
(64) Rydman, E. M.; Ilves, M.; Koivisto, A. J.; Kinaret, P.; Fortino, V.; Savinko, T. S.; Lehto, M. T.; Pulkkinen, V.; Vippola, M.; Hämeri, K. J.; et al. Inhalation of rod-like carbon nanotubes causes unconventional allergic airway inflammation. *Part. Fibre Toxicol.* **2014**, *11*, 48.
(65) Derewenda, U.; Li, J.; Derewenda, Z.; Dauter, Z.; Mueller, G.; Rule, G.; Benjamin, D. The Crystal Structure of a Major Dust Mite Allergen Der p 2, and its Biological Implications. *J. Mol. Biol.* **2002**, *318*, 189−197.
(66) Reginald, K.; Chew, F. The Major Allergen Der p 2 is a Cholesterol Binding Protein. *Sci. Rep.* **2019**, *9*, 1556.
(67) Roth-Walter, F.; Gomez-Casado, C.; Pacios, L. F.; Mothes-Luksch, N.; Roth, G. A.; Singer, J.; Diaz-Perales, A.; Jensen-Jarolim, E. Bet v 1 from Birch Pollen is a Lipocalin-Like Protein Acting as Allergen Only When Devoid of Iron by Promoting Th2 Lymphocytes. *J. Biol. Chem.* **2014**, *289*, 17416−17421.
(68) Roth-Walter, F.; Pacios, L. F.; Gomez-Casado, C.; Hofstetter, G.; Roth, G. A.; Singer, J.; Diaz-Perales, A.; Jensen-Jarolim, E. The Major Cow Milk Allergen Bos d 5 Manipulates T-Helper Cells Depending on its Load with Siderophore-Bound Iron. *PLoS One* **2014**, *9*, No. e104803.
(69) Angelina, A.; Sirvent, S.; Palladino, C.; Vereda, A.; Cuesta-Herranz, J.; Eiwegger, T.; Rodríguez, R.; Breiteneder, H.; Villalba, M.; Palomares, O. The Lipid Interaction Capacity of Sin a 2 and Ara h 1, Major Mustard and Peanut Allergens of the Cupin Superfamily, Endorses Allergenicity. *Allergy.* **2016**, *71*, 1284−1294.
(70) Kimata, H. Cholesterol Selectively Enhances *In Vitro* Latex-Specific IgE Production in Atopic Dermatitis Patients with Latex Allergy. *Life Sci.* **2005**, *76*, 1527−1532.
(71) McKay, A.; Leung, B. P.; McInnes, I. B.; Thomson, N. C.; Liew, F. Y. A Novel Anti-Inflammatory Role of Simvastatin in a Murine Model of Allergic Asthma. *J. Immunol.* **2004**, *172*, 2903−2908.
(72) Wills-Karp, M.; Luyimbazi, J.; Xu, X.; Schofield, B.; Neben, T. Y.; Karp, C. L.; Donaldson, D. D. Interleukin-13: Central Mediator of Allergic Asthma. *Science* **1998**, *282* (5397), 2258−2261.
(73) Zhu, Z.; Homer, R. J.; Wang, Z.; Chen, Q.; Geba, G. P.; Wang, J.; Zhang, Y.; Elias, J. A. Pulmonary Expression of Interleukin-13 Causes Inflammation, Mucus Hypersecretion, Subepithelial Fibrosis, Physiologic Abnormalities, and Eotaxin Production. *J. Clin. Invest.* **1999**, *103* (6), 779−788.
(74) You, D. J.; Lee, H. Y.; Taylor-Just, A. J.; Linder, K. E.; Bonner, J. C. Sex Differences in the Acute and Subchronic Lung Inflammatory Responses of Mice to Nickel Nanoparticles. *Nanotoxicology* **2020**, *14*, 1058−1081.
(75) Melgert, B. N.; Postma, D. S.; Kuipers, I.; Geerlings, M.; Luinge, M. A.; van der Strate, B. W.; Kerstjens, H. A.; Timens, W.; Hylkema, M. N. Female Mice are More Susceptible to the Development of Allergic Airway Inflammation than Male Mice. *Clin. Exp. Allergy* **2005**, *35*, 1496−1503.
(76) Karkout, R.; Gaudreault, V.; Labrie, L.; Aldossary, H.; Azalde Garcia, N.; Shan, J.; Fixman, E. D. Female-Specific Enhancement of Eosinophil Recruitment and Activation in a Type 2 Innate Inflammation Model in the Lung. *Clin. Exp. Immunol.* **2023**, *216*, 13−24.
(77) Kurowska-Stolarska, M.; Stolarski, B.; Kewin, P.; Murphy, G.; Corrigan, C. J.; Ying, S.; Pitman, N.; Mirchandani, A.; Rana, B.; van Rooijen, N.; Shepherd, M.; McSharry, C.; McInnes, I. B.; Xu, D.; Liew, F. Y. IL-33 Amplifies the Polarization of Alternatively Activated Macrophages That Contribute to Airway Inflammation. *J. Immunol.* **2009**, *183*, 6469−6477.
(78) Beamer, C. A.; Girtsman, T. A.; Seaver, B. P.; Finsaas, K. J.; Migliaccio, C. T.; Perry, V. K.; Rottman, J. B.; Smith, D. E.; Holian, A. IL-33 Mediates Multi-Walled Carbon Nanotube (MWCNT)-Induced Airway Hyper-Reactivity Via the Mobilization of Innate Helper Cells in the Lung. *Nanotoxicology* **2013**, *7*, 1070−1081.
(79) Ray, J. L.; Holian, A. Sex Differences in the Inflammatory Immune Response to Multi-Walled Carbon Nanotubes and Crystalline Silica. *Inhal Toxicol.* **2019**, *31*, 285−297.
(80) Ray, J. L.; Shaw, P. K.; Postma, B.; Beamer, C. A.; Holian, A. Nanoparticle-Induced Airway Eosinophilia Is Independent of ILC2 Signaling but Associated with Sex Differences in Macrophage Phenotype Development. *J. Immunol.* **2022**, *208*, 110−120.
(81) Fukushima, S.; Kasai, T.; Umeda, Y.; Ohnishi, M.; Sasaki, T.; Matsumoto, M. Carcinogenicity of Multi-Walled Carbon Nanotubes: Challenging Issue on Hazard Assessment. *J. Occup. Health* **2018**, *60*, 10−30.
(82) Kim, K. H.; Kim, K. T.; Lee, S. K.; Park, H. S.; Lee, Y. M.; Nahm, D. H.; Son, C. H.; Yang, D. K.; Roh, M. S.; Choi, P. J.; Lee, J. H.; Kim, K. N.; Lee, K. N. Sensitization Rates for Inhalant Allergens in Patients with Respiratory Allergy in Busan. *Korean J. Asthma Allergy Clin. Immunol.* **2005**, *25*, 59−63.
(83) Lee, J. H.; Lee, S. B.; Bae, G. N.; Jeon, K. S.; Yoon, J. U.; Ji, J. H.; Sung, J. H.; Lee, B. G.; Lee, J. H.; Yang, J. S.; Kim, H. Y.; Kang, C. S.; Yu, I. J. Exposure Assessment of Carbon Nanotube Manufacturing Workplaces. *Inhalation Toxicol.* **2010**, *22*, 369−381.
(84) Dahm, M. M.; Evans, D. E.; Schubauer-Berigan, M. K.; Birch, M. E.; Fernback, J. E. Occupational Exposure Assessment in Carbon Nanotube and Nanofiber Primary and Secondary Manufacturers. *Ann. Occup. Hyg.* **2012**, *57*, 328−344.
(85) Schubauer-Berigan, M. K.; Dahm, M. M.; Erdely, A.; Beard, J. D.; Eileen Birch, M.; Evans, D. E.; Fernback, J. E.; Mercer, R. R.; Bertke, S. J.; Eye, T.; de Perio, M. A. Association of Pulmonary, Cardiovascular, and Hematologic Metrics with Carbon Nanotube and Nanofiber Exposure Among U.S. Workers: A Cross-Sectional Study. *Part. Fibre Toxicol.* **2018**, *15*, 22.
(86) Matuka, D. O.; Ratshikhopha, E.; Singh, T. House Dust Mites: Challenges with Establishing Causal Associations in Occupational Health for Ubiquitous Agents - A Retrospective Study. *Curr. Allergy Clin. Immunol.* **2023**, *36* (2), 106−117.

https://doi.org/10.1021/acsnano.4c07893
ACS Nano 2024, 18, 26215−26232